Tuning inter-modal energy exchanges of a nonlinear electromechanical beam by a nonlinear circuit

Vinciane Guillot, Alireza Ture Savadkoohi, Claude-Henri Lamarque

Noname manuscript No.
(will be inserted by the editor)

Tuning inter-modal energy exchanges of a nonlinear electromechanical beam by a nonlinear circuit

V. Guillot · A. Ture Savadkoohi · C.-H. Lamarque

Received: date / Accepted: date

Abstract A model of a nonlinear beam with a piezoelectric patch linked to a nonlinear circuit is considered. The physical and mechanical parameters of the system are such that it presents a 1:3 internal resonance. The aim is to study, for different time scales, the effect of the nonlinearity of the electrical circuit on energy exchanges between the resonant modes. In fact, we would like to master energy channelling between two internally resonant modes of a composite beam via a nonlinear circuit. The investigations are carried out on the projected system equations on its internally resonant modes. The system behaviours at different scales of time are studied by coupled methods of complexification and multiple scale. Analytical developments permit to reveal different system dynamics characterized by periodic and/or non periodic regimes. Finally, the paper is accompanied by comparisons between systems equipped with a resonant circuit (linear) and a nonlinear one.

Keywords nonlinear dynamics · piezoelectric patch · inter-modal energy exchanges · internal resonance · nonlinear circuit

1 Introduction

Nonlinear vibrations of structural systems have been widely studied over the years with the aim of mitigating or harvesting their energies [1,2,3]. Depending on the geometrical characteristic of nonlinear beams and also on the nature of external excitations, they can present different types of internal or combination or auto parametric resonances [4,5,6,7,8,9]. It can be shown that via developing nonlinear equations of a cantilevered beam until third order, one can reach to cubic nonlinear terms [10,11]. Several types of internal resonances can be observed [12, 6] including a $1:3$ internal resonance, meaning that two natural frequencies of

V. Guillot, A. Ture Savadkoohi, C.-H. Lamarque
Univ Lyon, ENTPE, LTDS UMR CNRS 5513
3 Rue Maurice Audin 69518 Vaulx-en-Velin Cedex, France
Tel.: +33 4 72 04 72 46
E-mail: alireza.turesavadkoohi@entpe.fr

the system (ω_m and ω_n) are positioned in such a way that: $\omega_m \simeq 3\omega_n$. It is shown that different strategies can be used to tune natural frequencies presenting a certain ratio, e.g. via imposing a particular cross-section [5]. In previous works, it is proven that via patching piezoelectric materials at special positions on the beam, a $1:2$ and also a $1:3$ internal resonances can be achieved [13,14].
Piezoelectric materials can be used in order to mitigate or to harvest vibratory energies [15,3]. The effectiveness of a piezoelectric patches to achieve the desired outcome (energy harvesting or vibration mitigation) can be increased through its electrical components. Indeed, the electrical components of the circuits linked to the piezoelectric materials can be optimized according to design purposes [16]. Different electrical circuits have been proposed and studied over the years, e.g. classical circuits as resistive circuits (composed of a simple resistance) [17] or resonant ones (composed of a capacitance and a resistance) [18]. Moreover, nonlinear circuits have been implemented to extend the frequency range of application of systems, such as a nonsmooth nonlinearity created through switch devices [19,20, 21,22] or cubic nonlinearity due to nonlinear capacitance devices [23] and electrical networks [24]. Usually, most of designs aim at periodic responses of the system and piezoelectric materials are used to reduce the vibration of one special mode, or several piezoelectric materials are patched to mitigate the vibrations of several modes of the structure [25,26]. So, the overall electromechanical system can be used as a nonlinear absorber as in mechanical systems [27,28,29,30,31,32,33,34, 35,36].
Our previous developments devoted to the creation of an energy exchange between the second and third modes of an electromechanical system due to a $1:3$ internal resonance [13,14]. This nonlinear behaviour was produced by the inherent nonlinearities of the electromechanical system. Then, we studied the possibility of using an adaptable nonlinear circuit when the system originally does not present any internal resonance [37]: It was shown that the components of the nonlinear circuit can be tuned to obtain desired dynamical behaviours of the system. This article is dealing with the use of an adaptable nonlinear circuit to master an inter-modal energy exchanges between two resonant modes of an electromechanical structure.
Organization of the paper is as it follows: The composite system and its governing equations are presented in Sect. 1. The projection of the system on its internally resonant modes is illustrated at the same section. Analytical treatments of the system via classical multiple scale method is presented in Sect. 2. Then, in Sect. 3, the complexification / multiple scale methods are exploited for detection of the fast and slow system dynamics. Finally, the paper is concluded in Sect.4.

2 Presentation of the composite system

The system is composed of a homogeneous beam patched with a single piezoelectric material. The patch has the fixed length (L_p) and width b equal to the width of the beam, and is positioned between $x = x_1$ and $x = x_2$, see Fig. 1. Originally a three-dimensional Euler-Bernoulli beam model is developed: It is assumed that the beam can present large deformations, preserving a nonlinear elastic behaviour, while the cross sections remains straight. The neutral axis of the beam is supposed to be inextensible. Then, after derivation of the Green's strain tensor of the beam and obtaining the Lagrangian, governing system equations are developed until

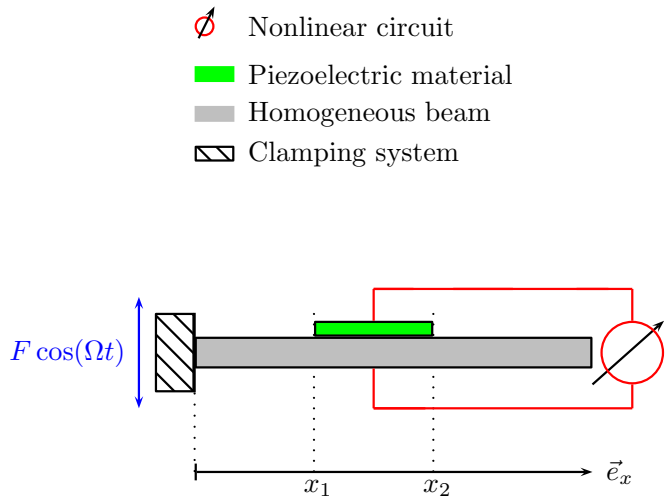

Fig. 1 Scheme of the composite system: a homogeneous beam is patched with a piezoelectric material at $x \in [x_1, x_2]$. The piezoelectric material is coupled to a nonlinear circuit. The overal system is under lateral base excitation as $F\cos(\Omega t)$.

the third order nonlinearities. For the piezoelectric patch, we suppose a linear behaviour of piezoelectric material [38] and we ignore its nonlinear terms [13,39, 40]. Moreover, we suppose it has same displacement as the homogeneous beam during the deformation. Governing systems equations after detailed developments of [41] read as:

$$\begin{aligned}\mu\ddot{v} + c_v\dot{v} - \mu F\Omega^2\cos(\Omega t) = \Bigg[& -EI(v'''' + v'(v'v'')') \\ & + v'\int_s^{L_b} -\frac{\mu}{2}\int_s^0 \ddot{(v'^2)}\, ds\, ds \\ & -(\delta(s-x_1) - \delta(s-x_2))\frac{b_p d_{31}(y_2^2 - y_1^2)}{2h_p}V\Bigg]'\end{aligned} \tag{1}$$

$$q = \int_{x_1}^{x_2} \left(b_p d_{31}(y_2 - y_1)v'' + \frac{b_p\varepsilon_{33}}{h_p}V\right)\, ds \tag{2}$$

with μ, c_v, EI the mass density, the damping, the Young modulus and inertia of the system. V , q are the electrical tension and the electrical charge of the piezoelectric material, respectively. The system is under base excitation as $F\cos(\Omega t)$, where F is the amplitude of the lateral base excitation with the driving frequency of Ω. b_p and h_p are the width and the thickness of the piezoelectric material. d_{31}, ε_{33}, y_2 and y_1 are the piezoelectric coefficient, the permittivity and the positions of the electrodes of the piezoelectric material with respect to the neutral axis (see Fig. 2). x_1 and x_2 give the position of the piezoelectric patch. Let us assume that the system presents a $1:3$ internal resonance between the n^{th} and m^{th} modes. Thus, the spatio-temporal variable $v(s,t)$ is supposed to take the following form:

$$v(s,t) = \phi_n(s)r_n(t) + \phi_m(s)r_m(t) \tag{3}$$

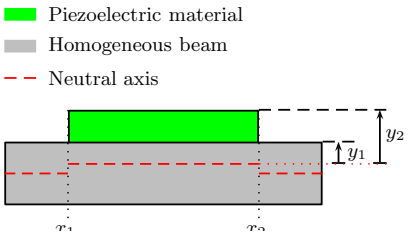

Fig. 2 Positions of electrodes of the piezoelectric material with respect to the neutral axis (y_1 and y_2).

Through the projection of the Eq. 1 on n^{th} and m^{th} modes, we obtain:

$$\begin{aligned}
\ddot{r}_n + \mu_n \dot{r}_n + \omega_n^2 r_n = {} & De_{nnn} r_n^3 + De_{nnm} r_n^2 r_m \\
& + De_{nmm} r_n r_m^2 + De_{mmm} r_m^3 \\
& + 2(G_{nnn} r_n + G_{mnn} r_m)(\dot{r}_n^2 + r_n \ddot{r}_n) \\
& + (G_{nnm} r_n + G_{mnm} r_m)(\ddot{r}_n r_m + 2\dot{r}_n \dot{r}_m + r_n \ddot{r}_n) \\
& + 2(G_{nmm} r_n + G_{mmm} r_m)(\dot{r}_m^2 + r_m \ddot{r}_m) \\
& + De_V \; V - F_n \Omega^2 \cos(\Omega t) \\
\ddot{r}_m + \mu_m \dot{r}_m + \omega_m^2 r_m = {} & Ae_{nnn} r_n^3 + Ae_{nnm} r_n^2 r_m \\
& + Ae_{nmm} r_n r_m^2 + Ae_{mmm} r_m^3 \\
& + 2(Ga_{nnn} r_n + Ga_{mnn} r_m)(\dot{r}_n^2 + r_n \ddot{r}_n) \\
& + (Ga_{nnm} r_n + Ga_{mnm} r_m)(\ddot{r}_n r_m + 2\dot{r}_n \dot{r}_m + r_n \ddot{r}_n) \\
& + 2(Ga_{nmm} r_n + Ga_{mmm} r_m)(\dot{r}_m^2 + r_m \ddot{r}_m) \\
& + Ae_V \; V - F_m \Omega^2 \cos(\Omega t)
\end{aligned} \tag{4}$$

Different system coefficients are defined in Appendix A. The electrical tension V is expressed as:

$$V = \frac{1}{L_V}(q - L_n r_n - L_m r_m) \tag{5}$$

with:

$$\begin{aligned}
L_V &= \frac{b_p d_{31}(y_2^2 - y_1^2)(x_2 - x_1)}{2h_p} \\
L_n &= \int_{x_1}^{x_2} b_p d_{31}(y_2 - y_1)\phi_n''(s)\, ds \\
L_m &= \int_{x_1}^{x_2} b_p d_{31}(y_2 - y_1)\phi_m''(s)\, ds
\end{aligned} \tag{6}$$

Supposing a nonlinear electrical circuit composed of an inductance L_0, a resistance R, a negative capacitance C_{neg} and a nonlinear capacitance C_{NL}, the electrome-

Table 1 Mechanical parameters of the beam

ρ_b (kg/m^3)	E_b (Pa)	h_b (mm)	b (mm)	L_b (m)
$9\ 10^3$	$105\ 10^9$	0.5	30	0.18

Table 2 Mechanical and material parameters of the piezoelectric patch. C/N stands for Coulomb/Newton.

ρ_p (kg/m^3)	E_p (Pa)	h_p (mm)	d_{31} (C/N)	ε_{33} (C/N)	b (mm)
7650	$93.8\ 10^9$	0.2	10.13	$-9.08\ 10^{-9}$	30

chanical equation of the circuit (see Eq. 2) reads:

$$L_0\ddot{q} + R\dot{q} + \frac{1}{C_{NL}}q^3 + \frac{1}{C_{neg}}q = \frac{1}{L_V}(q - L_n r_n - L_m r_m) \tag{7}$$

To nondimensionalize the equations, we set:

$$t^* = \omega_n t \tag{8}$$

Then, following system of equations are obtained in time domaine t^*:

$$\begin{aligned}
&\ddot{r}_n + a_1\dot{r}_n + r_n = \\
&\Lambda_{nnn}r_n^3 + \Lambda_{nnm}r_n^2 r_m + \Lambda_{nmm}r_n r_m^2 + \Lambda_{mmm}r_m^3 + \gamma_V q + \gamma_n r_n + \gamma_m r_m \\
&+2(L_{nnn}r_n + L_{mnn}r_m)(\dot{r}_n^2 + r_n\ddot{r}_n) \\
&+(L_{nnm}r_n + L_{mnm}r_m)(\ddot{r}_n r_m + 2\dot{r}_n\dot{r}_m + r_n\ddot{r}_n) \\
&+2(L_{nmm}r_n + L_{mmm}r_m)(\dot{r}_m^2 + r_m\ddot{r}_m) - F_n\nu^2\cos(\nu t^*) \\
&\\
&\ddot{r}_m + a_2\dot{r}_m + (\frac{\omega_m}{\omega_\eta})^2 r_m = \\
&\Gamma_{nnn}r_n^3 + \Gamma_{nnm}r_n^2 r_m + \Gamma_{nmm}r_n r_m^2 + \Gamma_{mmm}r_m^3 + \beta_V q + \beta_n r_n + \beta_m r_m \\
&+2(T_{nnn}r_n + T_{mnn}r_m)(\dot{r}_n^2 + r_n\ddot{r}_n) \\
&+(T_{nnm}r_n + T_{mnm}r_m)(\ddot{r}_n r_m + 2\dot{r}_n\dot{r}_m + r_n\ddot{r}_n) \\
&+2(T_{nmm}r_n + T_{mmm}r_m)(\dot{r}_m^2 + r_m\ddot{r}_m) - F_m\nu^2\cos(\nu t^*) \\
&\\
&\ddot{q} + a_3\dot{q} + \gamma q^3 = \Theta_V q + \Theta_n r_n + \Theta_m r_m
\end{aligned} \tag{9}$$

where $\nu = \dfrac{\Omega}{\omega_n}$ and other system parameters are defined in Appendix A (note that $\Theta_V < 0$).
In the next section, the mechanical and geometrical properties of the composite are presented. The physical and mechanical properties of the coupled structure are chosen in a manner that it presents a $1:3$ internal resonance between two of its modes [13,14].

2.1 Parameters of the composite

The mechanical and material parameters of the coupled system are reported in Tabs 1 and 2. In order to obtain the $1:3$ internal resonance, it is supposed that the piezoelectric patch is placed in $x_1 = 0.031$ m and $x_2 = 0.081$ m. This position is chosen according to the method explained in [13]. In this case, the second (ω_2) and

Table 3 Second and third natural pulsations of the composed system and their ratio

ω_2 (rad/s)	ω_3 (rad/s)	ω_3/ω_2
342.8	1030	3.005

the third (ω_3) natural frequencies of the system present a $1:3$ internal resonance, see Tab. 3. It has been shown that this internal resonance leads to vibratory energy exchanges between two mentioned modes due to the inherent nonlinearities of the electromechanical system [14]. The mechanical parameters being known, only the electrical parameters of the nonlinear circuit remain to be tuned.
In the next section a classical multiple scale method is endowed for detecting periodic regimes of the system.

3 Analytical treatments of system of equations via the direct multiple scale method

To implement the multiple scale method [42], a small book-keeping parameter ϵ is considered, allowing the definition of different times scales as it follows:

$$t_i = \epsilon^i \; t^*, \; i = 1, ..., n \tag{10}$$

t_0 is the fast time scale and t_1, ..., t_n are different slow time scales. This lead to:

$$D_i = \frac{\partial}{\partial t_i}, \; i = 0, 1, .. \tag{11}$$

Moreover, we assume that following system parameters are $\mathcal{O}(\epsilon)$: a_1, a_2, F_n, F_m, γ_V, γ_n, γ_m, β_V, β_n, β_m, γ, and also all parameters linked to cubic terms. In further analytical developments the scaled parameters with respect to the ϵ parameter are represented by addition of the index 0 to the original version such as, $a_1 = \epsilon \; a_{10}$, $F_n = \epsilon \; F_{n0}$, etc. With mentioned assumptions, modes and the nonlinear circuit are weakly coupled while the circuit itself is weakly nonlinear (see Eq. 9).
As for the time variables r_n, r_m and q, they are written as:

$$\begin{aligned} r_n &= r_{n0} + \epsilon r_{n1} + ... \\ r_m &= r_{m0} + \epsilon r_{m1} + ... \\ q &= q_0 + \epsilon q_1 + ... \end{aligned} \tag{12}$$

Since a $1:3$ internal resonance is created between the second and third modes ($m = 3$, $n = 2$), it is supposed that:

$$\frac{\omega_m}{\omega_n} = 3 + \sigma_2 \epsilon \tag{13}$$

with σ_2 a detuning parameter linked to the realization of the $1:3$ internal resonance.
The driving frequency of excitation ν is supposed to be:

– around the lower mode (ω_n) as:

$$\nu = 1 + \sigma \epsilon \tag{14}$$

– or around the higher mode (ω_m) as:

$$\nu = 3 + \tilde{\sigma}\epsilon \tag{15}$$

The explained methodology in [13] is exploited step by step. Let us consider different orders of ϵ of governing system equations.
Equation 9 at $\mathcal{O}(1)$ reads:

$$\begin{array}{l} {D_0}^2 r_{n0} + r_{n0} = 0 \\ {D_0}^2 r_{m0} + 9 r_{m0} = 0 \\ {D_0}^2 q_0 + a_3 D_0 q_0 = \Theta_{m0} r_{m0} + \Theta_{n0} r_{m0} + \Theta_{V0} q_0 \end{array} \tag{16}$$

So,

$$\begin{array}{l} r_{n0} = A_n \exp(it_0) + \overline{A}_n \exp(-it_0) \\ r_{m0} = A_m \exp(3it_0) + \overline{A}_m \exp(-3it_0) \\ q_0 = \mathcal{L}_{1n} \exp(it_0) + \mathcal{L}_{1m} \exp(3it_0) + cc \end{array} \tag{17}$$

with:

$$\begin{array}{l} \mathcal{L}_{1n} = \dfrac{-\Theta_{n0}(1 + ia_3 + \Theta_{V0})}{a_3^2 + (1 + \Theta_{V0})^2} \\ \\ \mathcal{L}_{1m} = \dfrac{-\Theta_{m0}(9 + 3ia_3 + \Theta_{V0})}{9a_3^2 + (9 + \Theta_{V0})^2} \end{array} \tag{18}$$

At $\mathcal{O}(\epsilon)$,

– for ν around 1 (see Eq. 14), the first two equations of the system 9 become:

$$\begin{array}{l} D_0^2 r_{n1} + r_{n1} = L_{nnn0} {r_{n0}}^3 + L_{nnm0} r_{n0}^2 r_{m0} + L_{nmm0} r_{n0} r_{m0}^2 \\ + L_{mmn0} r_{m0}^3 + 2G_{mmm0} \left((D_0 r_{m0})^2 + r_{m0} D_0^2 r_{m0} \right) r_{m0} - a_{10} D_0 r_{n0} \\ - 2D_1 D_0 r_{n0} + G_{mnm0} r_{m0} (r_{n0} D_0^2 r_{m0} + D_0 r_{n0} D_0 r_{m0} + r_{m0} D_0^2 r_{n0}) \\ + 2G_{nmm0} \left((D_0 r_{m0})^2 + r_{m0} D_0^2 r_{m0} \right) r_{n0} \\ + G_{nnm0} r_{n0} (r_{n0} D_0^2 r_{m0} + D_0 r_{n0} D_0 r_{m0} + r_{n0} D_0^2 r_{m0}) \\ + 2G_{nnn0} \left((D_0 r_{n0})^2 + r_{n0} D_0^2 r_{n0} \right) r_{n0} \\ + 2G_{mnn0} \left((D_0 r_{n0})^2 + r_{n0} D_0^2 r_{n0} \right) r_{m0} + \gamma_{n0} r_{n0} + \gamma_{m0} r_{m0} + \gamma_{V0} q_0 \\ - \dfrac{1}{2} F_{n0} (e^{it_0 + i\sigma t_1} + e^{-it_0 - i\sigma t_1}) \\ \\ D_0^2 r_{m1} + 9 r_{m1} = 2G_{annn0} \left((D_0 r_{n0})^2 + r_{n0} D_0^2 r_{n0} \right) r_{n0} \\ + 2G_{ammm0} r_{m0} (D_0 r_{m0}^2 + r_{m0} D_0^2 r_{m0}) \\ + G_{amnm0} r_{m0} (r_{n0} D_0^2 r_{m0} + D_0 r_{n0} D_0 r_{m0} + r_{m0} D_0^2 r_{n0}) \\ + 2G_{anmm0} \left((D_0 r_{m0})^2 + r_{m0} D_0^2 r_{m0} \right) r_{n0} \\ + 2G_{amnn0} \left((D_0 r_{n0})^2 + r_{n0} D_0^2 r_{n0} \right) r_{m0} \\ + G_{annm0} r_{n0} (r_{n0} D_0^2 r_{m0} + D_0 r_{n0} D_0 r_{m_0} + r_{m0} D_0^2 r_{n0}) - 6 r_{m0} \sigma_2 \\ + T_{mmm0} r_{m0}^3 + T_{nmm0} r_{n0} r_{m0}^2 + T_{nnm0} r_{m0} r_{n0}^2 + T_{nnn0} r_{n0}^3 \\ - 2D_1 D_0 r_{m0} + \beta_{V0} q_0 + \beta_{m0} r_{m0} + \beta_{n0} r_{n0} - a_{20} D_0 r_{m0} \\ - \dfrac{1}{2} F_{m0} (e^{it_0 + i\sigma t_1} + e^{-it_0 - i\sigma t_1}) \end{array} \tag{19}$$

Cancellation of secular terms of Eq. 19 provides:

$$\begin{aligned}
2iD_1A_n = & -\frac{1}{2}F_{n0}\exp(i\sigma t_1) + \gamma_{n0}A_n - ia_{10}A_n + \gamma_{V0}\mathcal{L}_{1n}A_n \\
& +2(L_{nmm0} - 9(G_{nmn0} + G_{nnm0}))A_nA_m\overline{A}_m \\
& +(L_{nnm0} - 4G_{mnn0} - 6G_{nnm0})A_m\overline{A}_n^2 \\
& +(3L_{nnn0} - 4G_{nnn0})A_n^2\overline{A}_n \\
6iD_1A_m = & \gamma_{m0}A_m - 3ia_{20}A_m - 6\sigma_2A_m + \beta_{V0}\mathcal{L}_{1m}A_m \\
& +3(T_{mmm0} - 12Ga_{mmm0} - 9Ga_{mnm0})A_m^2\overline{A}_m \\
& +2(T_{nnm0} - 9Ga_{nnm0})A_mA_n\overline{A}_n \\
& +(T_{nnn0} - 4Ga_{nnn0})A_n^3
\end{aligned} \tag{20}$$

To eliminate the time scale t_1 from equations and to find algebraic systems from the real and imaginary parts, it is supposed (with $i^2 = -1$):

$$\begin{aligned}
A_n &= (p_n + iq_n)\exp(i\sigma t_1) \\
A_m &= (p_m + iq_m)\exp(3i\sigma t_1)
\end{aligned} \tag{21}$$

with $(p_n, q_n, p_m, q_m) \in \mathbb{R}$.
Then, to find the amplitude of the first harmonic of r_m, the particular solution of r_{m1} is found as:

$$r_{m1}(t_0) = M_1\exp(it_0) + cc \tag{22}$$

– for ν around 3 (see Eq. 15), the first two equations of the system 9 read:

$$\begin{aligned}
& D_0^2r_{n1} + r_{n1} = L_{nnn0}{r_{n0}}^3 + L_{nnm0}r_{n0}^2r_{m0} + L_{nmm0}r_{n0}r_{m0}^2 \\
& +L_{mmm0}r_{m0}^3 + 2G_{mmm0}\left((D_0r_{m0})^2 + r_{m0}D_0^2r_{m0}\right)r_{m0} - a_{10}D_0r_{n0} \\
& -2D_1D_0r_{n0} + G_{mnm0}r_{m0}(r_{n0}D_0^2r_{m0} + D_0r_{n0}D_0r_{m0} + r_{m0}D_0^2r_{n0}) \\
& +2G_{nmm0}\left((D_0r_{m0})^2 + r_{m0}D_0^2r_{m0}\right)r_{n0} \\
& +G_{nnm0}r_{n0}(r_{n0}D_0^2r_{m0} + D_0r_{n0}D_0r_{m0} + r_{n0}D_0^2r_{m0}) \\
& +2G_{nnn0}\left((D_0r_{n0})^2 + r_{n0}D_0^2r_{n0}\right)r_{n0} \\
& +2G_{mnn0}\left((D_0r_{n0})^2 + r_{n0}D_0^2r_{n0}\right)r_{m0} + \gamma_{V0}q_0 + \gamma_{m0}r_{m0} + \gamma_{n0}r_{n0} \\
& -\frac{9}{2}F_{n0}e^{3it_0+3i\tilde{\sigma}t_1} + e^{-3it_0-3i\tilde{\sigma}t_1}) \\
& D_0^2r_{m1} + 9r_{m1} = 2G_{annn0}\left((D_0r_{n0})^2 + r_{n0}D_0^2r_{n0}\right)r_{n0} \\
& +2G_{ammm0}r_{m0}(D_0r_{m0}^2 + r_{m0}D_0^2r_{m0}) \\
& +G_{amnm0}r_{m0}(r_{n0}D_0^2r_{m0} + D_0r_{n0}D_0r_{m0} + r_{m0}D_0^2r_{n0}) \\
& +2G_{anmm0}\left((D_0r_{m0})^2 + r_{m0}D_0^2r_{m0}\right)r_{n0} \\
& +2G_{amnn0}\left((D_0r_{n0})^2 + r_{n0}D_0^2r_{n0}\right)r_{m0} \\
& +G_{annm0}r_{n0}(r_{n0}D_0^2r_{m0} + D_0r_{n0}D_0r_{m_0} + r_{m0}D_0^2r_{n0}) - 6r_{m0}\sigma_2 \\
& +T_{mmm0}r_{m0}^3 + T_{nmm0}r_{n0}r_{m0}^2 + T_{nnm0}r_{m0}r_{n0}^2 + T_{nnn0}r_{n0}^3 \\
& -2D_1D_0r_{m0} + \beta_{V0}q_0 + \beta_{m0}r_{m0} + \beta_{n0}r_{n0} - a_{20}D_0r_{m0} \\
& -\frac{9}{2}F_{m0}(e^{3it_0+3i\tilde{\sigma}t_1} + e^{-3it_0-3i\tilde{\sigma}t_1})
\end{aligned} \tag{23}$$

The secular terms of Eq. 23 verify:

$$\begin{aligned}
2iD_1A_n = \; & 2\gamma_{n0}A_n - ia_{10}A_n + \gamma_{V0}\mathcal{L}_{1n}A_n \\
& +2(L_{nmm0} - 9(G_{nmn0} + G_{nnm0}))A_nA_m\overline{A}_m \\
& +(L_{nnm0} - 4G_{mnn0} - 6G_{nnm0})A_m\overline{A}_n^2 \\
& +(3L_{nnn0} - 4G_{nnn0})A_n^2\overline{A}_n \\
6iD_1A_m = \; & -\frac{9}{2}F_{m0} + 6\gamma_{m0}A_m - 3ia_{20}A_m - 6\sigma_2A_m + \beta_{V0}\mathcal{L}_{1m}A_m \\
& +3(T_{mmm0} - 12Ga_{mmm0} - 9Ga_{mnm0})A_m^2\overline{A}_m \\
& +2(T_{nnm0} - 9Ga_{nnm0})A_mA_n\overline{A}_n \\
& +(T_{nnn0} - 4Ga_{nnn0})A_n^3
\end{aligned} \tag{24}$$

For eliminating the time t_1 and obtaining algebraic equations, it is supposed that:

$$\begin{aligned}
A_n = \; & (p_n + iq_n)\exp(\frac{1}{3}i\sigma t_1) \\
A_m = \; & (p_m + iq_m)\exp(i\sigma t_1)
\end{aligned} \tag{25}$$

with $(p_n, q_n, p_m, q_m) \in \mathbb{R}$.
To obtain the main harmonic of r_n, the particular solution r_{n1} reads:

$$r_{n1}(t_0) = N_1\exp(3it_0) + cc \tag{26}$$

The algebraic equations of the steady state responses are detected via setting:

$$\begin{cases}
D_1p_n \; = 0 \\
D_1q_n \; = 0 \\
D_1p_m = 0 \\
D_1q_m = 0
\end{cases} \tag{27}$$

The remaining task will be the evaluation of roots of these equations for sweeping forcing amplitudes and/or driving frequency

3.1 A numerical example: comparisons

Results obtained from analytical developments via the multiple scale method are compared with those obtained from direct numerical integration of Eqs. 4 and 7 with the ode45 function of Matlab. Figures 3 and 4 collect frequency response curves of different system variables for sweeping ν around 1 and 3, respectively. In these figures, amplitudes of the first and/or the third harmonics of system variables are considered. It is seen that for the case of ν varying around 1 (see Fig. 3), first harmonics of r_n and q provide good approximations of system responses, while for r_m, the third harmonic should be considered as well. For ν varying around 3 (see Fig. 4), first harmonics of all system variables provide good predictions of the system behaviours. In the next section a complexification technique accompanied by the multiple scale method is carried out in order to have a deeper vision about possible system behaviours, i.e. periodic and/or non periodic ones.

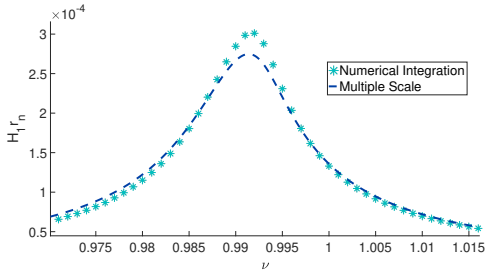

(a) Amplitude of the first harmonic of $r_n(t^*)$ obtained from: direct numerical integration of Eq. 9 ("*"); the multiple scale method ("- -").

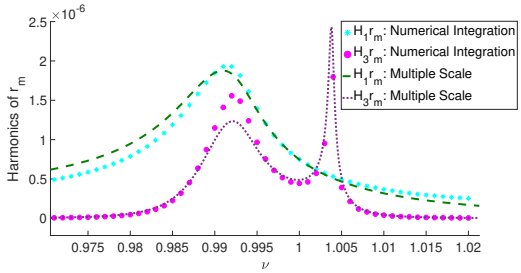

(b) Amplitude of the first and third harmonic of $r_m(t^*)$ obtained from: direct numerical integration of Eq. 9 ("*" and "o", respectively); the multiple scale method (see Eq. 27) ("- -" and ". .", respectively).

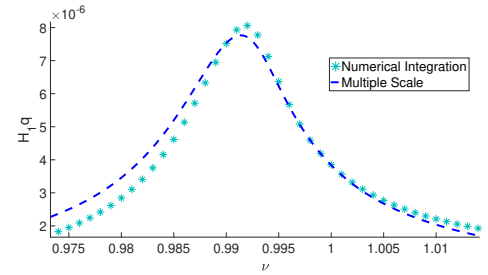

(c) Amplitude of the first harmonic of $q(t^*)$ obtained from: direct numerical integration of Eq. 9 ("*"); the multiple scale method (see Eq. 27) ("- -").

Fig. 3 The frequency response curves : the electrical parameters used are $R = 3050\ \Omega$ $L_0 =$ 106 Henry (H), $C_{NL} = 10^-15\ C^3/V$ and the forcing is $F = 7 \times 10^{-6}\ m$.

4 Analytical treatments of system of equations via complexification and multiple scale methods

Let us introduce following complexified variables to the system of Eq. 9 [43]:

$$\begin{aligned} &\dot{r}_n + i\nu r_n = \phi \exp(i\nu t^*) \\ &\dot{r}_m + 3i\nu r_m = \phi_3 \exp(3i\nu t^*) \\ &\dot{q} + i\nu q = \psi \exp(i\nu t^*) \end{aligned} \tag{28}$$

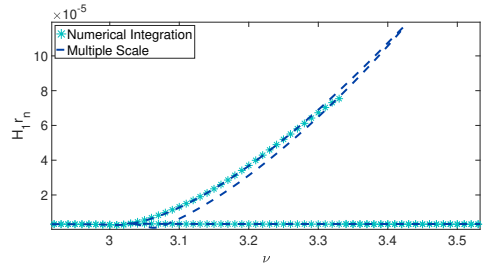

(a) Amplitude of the first harmonic of $r_n(t^*)$ obtained from: direct numerical integration of Eq. 9 ("*");the multiple scale method (see Eq. 27) ("- -").

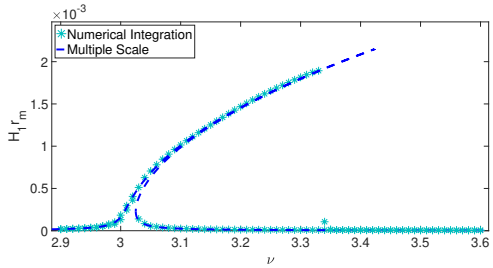

(b) Amplitude of the first harmonic of $r_m(t^*)$ obtained from: direct numerical integration of Eq. 9 ("*");the multiple scale method (see Eq. 27) ("- -").

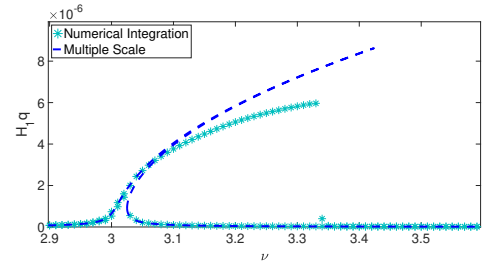

(c) Amplitude of the first harmonic of $q(t^*)$ obtained from: direct numerical integration of Eq. 9 ("*");the multiple scale method (see Eq. 27) ("- -").

Fig. 4 The frequency response curves: the electrical parameters used are $R = 3050\ \Omega$, $L_0 = 106\ H$, $C_{NL} = 10^-15\ C^3/V$ and the forcing is $F = 7 \times 10^{-6}\ m$.

It should be mentioned that in Eq. 28 only the third harmonics of variable r_m is considered. However, the problem can be extended to include its first harmonic and also to consider higher harmonics of system variables r_n, q as it is carried out in [44].

Let us consider a Galerking method, to take into account the first harmonics and to truncate higher ones. For an arbitrary function $\Xi(\phi, \phi_3, \psi)$, this is carried out

by:

$$\frac{\nu}{2\pi}\int_0^{\frac{2\pi}{\nu}} \Xi(\phi,\phi_3,\psi)\ \exp(-i\nu t^*)\ dt^* \tag{29}$$

In applying the integral of Eq. 29, it is supposed that ϕ, ϕ_3 and ψ are independent of the fast time scale. This will be checked during multiple scale method, where we will seek system responses when fast time leads to infinity.

– $\mathcal{O}(1)$ of system equations lead to:

$$\begin{aligned}
D_0\phi &= 0\\
D_0\phi_3 &= 0\\
D_0\psi &= \frac{1}{8\nu^3}(-4a_{30}\nu^3\psi + i(-4\nu^2\Theta_{n0}\phi - 4\nu^3\psi - 4\nu^2\Theta_{V0}\psi + 3\gamma_0\psi^2\overline{\psi}))\\
&= F(\phi,\overline{\phi},\psi,\overline{\psi})
\end{aligned} \tag{30}$$

Fixed points of the system impose that $D_0\psi = 0$ (where $t_0 \to \infty$), leading to the definition of the Slow Invariant Manifold (SIM) [45,46,47,48]:

$$\begin{aligned}
\phi &= \frac{1}{4\nu^2\Theta_n}(4i\nu^3 a_3\psi - 4\nu^4\psi - 4\nu^2\Theta_V\psi + 3\gamma\psi^2\overline{\psi})\\
&= f(\psi,\overline{\psi})
\end{aligned} \tag{31}$$

Here, the SIM is a geometrical bed for asymptotic states of the system which houses all equilibria of the system. In our study, the SIM is in fact a critical manifold of singularity perturbed fast-slow equations via $0 < \epsilon \ll 1$ parameter. This is very close to the definition of SIM which is described in [47]. Ginoux et al [46] and Ginoux [48] used the term SIM for wider aspects than critical manifolds. Classification and detailed discussions about most important techniques of detection of SIM namely, singular perturbation-based and curvature-based methods are provided by Ginoux [48].

– $\mathcal{O}(\epsilon)$ of system equations presents:

$$\begin{aligned}
D_1\phi &= \frac{1}{72\nu^3}(-2(18F_{n0}\nu^4 + 18a_{10}\nu^3\phi)\\
&\quad +i(-72\sigma\nu^3\phi + 2(10\nu^2 G_{mnm0} - 2L_{nmm0})\phi\phi_3\overline{\phi}_3\\
&\quad +(54\nu^2 G_{nnn0} - 27L_{nnn0})\phi^2\overline{\phi} +\\
&\quad +3(L_{nnm0} - 4\nu^2(G_{mnn0} + G_{nnm0}))\phi_3\overline{\phi}^2 - 36\nu^2\gamma_{V0}\psi))\\
&= G(\phi,\overline{\phi},\phi_3,\overline{\phi}_3,\psi,\overline{\psi})\\
D_1\phi_3 &= \frac{1}{72\nu^3}(-36a_{20}\nu^3\phi_3\\
&\quad +i(+(72\nu^3\sigma_2 - 12\nu^2\beta_{m0} - 216\nu^3\sigma)\phi_3\\
&\quad +9(T_{nnn0} - 4\nu^2 G a_{nnn0})\phi^3)\\
&\quad +(12\nu^2 G a_{mmm0} - T_{mmm0}\phi_3^2\overline{\phi}_3\\
&\quad +6(10\nu^2 G a_{nnm0} - T_{nnm0})\phi\overline{\phi}\phi_3))\\
&= H(\phi,\overline{\phi},\phi_3,\overline{\phi}_3)
\end{aligned} \tag{32}$$

We present the complex variables in polar domain as:

$$\begin{array}{l}\phi = N_1 \exp(i\delta_1)\\ \phi_3 = N_2 \exp(i\delta_2)\\ \psi = N_3 \exp(i\delta_3)\end{array} \tag{33}$$

with $(N_1, N_2, N_3) \in \mathbb{R}_+$ and $(\delta_1, \delta_2, \delta_3) \in \mathbb{R}$.
The real and imaginary parts of $F(\phi, \psi, \overline{\psi}) \exp(i\delta_3)$, $G(\phi, \overline{\phi}, \phi_3, \overline{\phi}_3, \psi) \exp(i\delta_1)$ and $H(\phi, \overline{\phi}, \phi_3, \overline{\phi}_3, \psi) \exp(i\delta_2)$ allow to find the expressions of $\cos(3\delta_1 - \delta_2)$, $\sin(3\delta_1 - \delta_2)$, $\cos(\delta_1 - \delta_3)$, $\sin(\delta_1 - \delta_3)$, $\cos(\delta_1)$ and $\sin(\delta_1)$.
From classical equation $\cos(\delta_1 - \delta_3)^2 + \sin(\delta_1 - \delta_3)^2 - 1 = 0$,following relation is obtained:

$$N_1 = \frac{N_3}{4\nu^2 \Theta_n} \sqrt{9\gamma^2 N_3^4 - 24\gamma\nu^2(\nu^2 + \theta_V)N_3^2 + 16\nu^4(a_3^2\nu^2 + (\nu^2 + \Theta_V)^2)} \tag{34}$$

And from $\cos(3\delta_1 - \delta_2)^2 + \sin(3\delta_1 - \delta_2)^2 - 1 = 0$ a polynomial equation of degree three in N_2^2 and N_1^2 is obtained, which lead to three-dimensioned definition of the SIM as a function of N_1, N_2 and N_3.
To obtain the extrema of the SIM, the Jacobian matrix $\boldsymbol{J}_0$ is defined as:

$$\boldsymbol{J}_0 = \begin{pmatrix} \dfrac{\partial f(\psi, \overline{\psi})}{\partial \psi} & \dfrac{\partial f(\psi, \overline{\psi})}{\partial \overline{\psi}} \\ \\ \dfrac{\partial \overline{f}(\psi, \overline{\psi})}{\partial \psi} & \dfrac{\partial \overline{f}(\psi, \overline{\psi})}{\partial \overline{\psi}} \end{pmatrix} \tag{35}$$

From $\det(\boldsymbol{J}_0) = 0$, the extreme points $N_{3,\pm}$ are found as:

$$N_{3,\pm} = \frac{2}{3\sqrt{\gamma}} \sqrt{2\nu^2(\nu^2 + \Theta_V) \pm \nu^2 \sqrt{(\nu^2 + \Theta_V)^2 - 3a_3^2\nu^2}} \tag{36}$$

From Eq. 34 $N_{1,\pm}$ can be obtained and from $\cos(3\delta_1 - \delta_2)^2 + \sin(3\delta_1 - \delta_2)^2 - 1 = 0$ the amplitudes of $N_{2,\pm}$ are established. Thus, the extreme points $(N_{1,\pm}, N_{2,\pm}, N_{3,\pm})$ can be totally identified.
Equilibrium points of the system are defined as (see Eqs. 30 and 32):

$$\begin{cases} D_0\psi = 0 \\ D_1\phi = 0 \\ D_1\phi_3 = 0 \end{cases} \Leftrightarrow \begin{cases} F(\phi, \overline{\phi}, \psi, \overline{\psi}) = 0 \\ G(\phi, \overline{\phi}, \phi_3, \overline{\phi}_3, \psi, \overline{\psi}) = 0 \\ H(\phi, \overline{\phi}, \phi_3, \overline{\phi}_3) = 0 \end{cases} \tag{37}$$

For detecting stable zones of the SIM, system variables are linearly perturbed as:

$$\begin{array}{l}\phi \ \ \rightarrow \phi + \Delta\phi\\ \phi_3 \rightarrow \phi_3 + \Delta\phi_3\\ \psi \ \ \rightarrow \psi + \Delta\psi\end{array} \tag{38}$$

with $|\Delta\phi| << |\phi|$, $|\Delta\phi_3| << |\phi_3|$ and $|\Delta\psi| << |\psi|$. Applying the perturbed form of complex variables in Eq. 30, following system is obtained:

$$\frac{\partial}{\partial \tau_0} \begin{pmatrix} \Delta\phi \\ \Delta\overline{\phi} \\ \Delta\phi_3 \\ \Delta\overline{\phi_3} \\ \Delta\psi \\ \Delta\overline{\psi} \end{pmatrix} = \begin{pmatrix} \boldsymbol{0} & \boldsymbol{0} & \boldsymbol{0} \\ \boldsymbol{0} & \boldsymbol{0} & \boldsymbol{0} \\ \boldsymbol{A} & \boldsymbol{0} & \boldsymbol{C} \end{pmatrix} \begin{pmatrix} \Delta\phi \\ \Delta\overline{\phi} \\ \Delta\phi_3 \\ \Delta\overline{\phi_3} \\ \Delta\psi \\ \Delta\overline{\psi} \end{pmatrix} \tag{39}$$

with the matrix $\boldsymbol{A}$ defined in Appendix B.
The sign of the real part of the eigenvalues of the $\boldsymbol{C}$ matrix defines stable/unstable zones of the SIM:

$$\boldsymbol{C} = \begin{pmatrix} \dfrac{\partial \mathcal{F}(\phi,\overline{\phi},\psi,\overline{\psi})}{\partial \psi} & \dfrac{\partial \mathcal{F}(\phi,\overline{\phi},\psi,\overline{\psi})}{\partial \overline{\psi}} \\ \dfrac{\partial \overline{\mathcal{F}}(\phi,\overline{\phi},\psi,\overline{\psi})}{\partial \psi} & \dfrac{\partial \overline{\mathcal{F}}(\phi,\overline{\phi},\psi,\overline{\psi})}{\partial \overline{\psi}} \end{pmatrix} \tag{40}$$

To perform stability analysis of equilibrium points at $\mathcal{O}(\epsilon)$, the system variables are perturbed as it is defined in Eq. 38. It reads as:

$$\frac{\partial}{\partial t_1}\begin{pmatrix} \Delta\phi \\ \Delta\overline{\phi} \\ \Delta\phi_3 \\ \Delta\overline{\phi_3} \\ \Delta\psi \\ \Delta\overline{\psi} \end{pmatrix} = \begin{pmatrix} \boldsymbol{M_1} & \boldsymbol{M_2} & \boldsymbol{M_3} \\ \boldsymbol{M_4} & \boldsymbol{M_5} & \boldsymbol{0} \\ \boldsymbol{0} & \boldsymbol{0} & \boldsymbol{0} \end{pmatrix} \begin{pmatrix} \Delta\phi \\ \Delta\overline{\phi} \\ \Delta\phi_3 \\ \Delta\overline{\phi_3} \\ \Delta\psi \\ \Delta\overline{\psi} \end{pmatrix} \tag{41}$$

Matricess M_j are defined in Appendix C.
Considering equation of the SIM in the form of $\phi = f(\psi,\overline{\psi})$, Eq. 41 yields to:

$$\frac{\partial}{\partial t_1}\begin{pmatrix} \Delta\psi \\ \Delta\overline{\psi} \\ \Delta\phi_3 \\ \Delta\overline{\phi_3} \end{pmatrix} = \boldsymbol{J}_1^{-1}\boldsymbol{M}^* \begin{pmatrix} \Delta\psi \\ \Delta\overline{\psi} \\ \Delta\phi_3 \\ \Delta\overline{\phi_3} \end{pmatrix} \tag{42}$$

with:

$$\boldsymbol{J}_1 = \begin{pmatrix} \dfrac{\partial f(\psi,\overline{\psi})}{\partial \psi} & \dfrac{\partial f(\psi,\overline{\psi})}{\partial \overline{\psi}} & 0 & 0 \\ \dfrac{\partial \overline{f}(\psi,\overline{\psi})}{\partial \psi} & \dfrac{\partial \overline{f}(\psi,\overline{\psi})}{\partial \overline{\psi}} & 0 & 0 \\ 0 & 0 & 1 & 0 \\ 0 & 0 & 0 & 1 \end{pmatrix} \tag{43}$$

and:

$$\boldsymbol{M}^* = \begin{pmatrix} \dfrac{\partial G}{\partial \phi_3} & \dfrac{\partial G}{\partial \overline{\phi}_3} & \dfrac{\partial G}{\partial \psi} & \dfrac{\partial G}{\partial \overline{\psi}} \\ \dfrac{\partial \overline{G}}{\partial \phi_3} & \dfrac{\partial \overline{G}}{\partial \overline{\phi}_3} & \dfrac{\partial \overline{G}}{\partial \psi} & \dfrac{\partial \overline{G}}{\partial \overline{\psi}} \\ \dfrac{\partial H}{\partial \phi_3} & \dfrac{\partial H}{\partial \overline{\phi}_3} & \dfrac{\partial H}{\partial \psi} & \dfrac{\partial H}{\partial \overline{\psi}} \\ \dfrac{\partial \overline{H}}{\partial \phi_3} & \dfrac{\partial \overline{H}}{\partial \overline{\phi}_3} & \dfrac{\partial \overline{H}}{\partial \psi} & \dfrac{\partial \overline{H}}{\partial \overline{\psi}} \end{pmatrix} \tag{44}$$

Studying above mentioned fast and slow dynamics of the system [49] leads to tracing periodic or non periodic regimes (e.g. modulated responses). The latter is governed by the existence of fold singularities which verify following conditions:

$$\begin{cases} F(\phi, \overline{\phi}, \psi, \overline{\psi}) = & 0 \\ G(\phi, \overline{\phi}, \phi_3, \overline{\phi}_3, \psi, \overline{\psi}) = & 0 \\ H(\phi, \overline{\phi}, \phi_3, \overline{\phi}_3) = & 0 \\ \det(\boldsymbol{J}_0) = 0 \end{cases} \tag{45}$$

Those are defined by $N_{1,\pm}, N_{2,\pm}, N_{3,\pm}$ associated to forcing amplitudes $F_{\pm}$. Different system regimes can be predicted via analysing following items:

- Effect of the components of the nonlinear electrical circuit on the system behaviours: This includes modification of the SIM and also existence of possible chaotic regimes if the linear part of the electrical equation becomes negative.
- Singular points and also equilibrium points (stable or unstable) leading to periodic or quasi-periodic solutions: This will depend on the position of the equilibrium points on the SIM and on the applied forcing amplitude F, for a fixed ν.
- The frequency response functions that are linked to periodic or quasi-periodic solutions for a sweeping frequency ν and or forcing amplitude F.

In the next section, first of all the effects of the components of the nonlinear electrical circuit are shown. Then results obtained from the direct integrations of the system of Eq. 9 by ode45 function of Matlab are compared with the analytically obtained results.

4.1 Numerical examples: effect of the electrical components

It can be seen from Eq. 34 that electrical components affect the geometry of the SIM. This will lead to identify effects of these parameters on the behaviour of the electromechanical system [37]. There is a critical value of the inductance L_0 which divides the geometry of the SIM into monotone and non monotone [37]. This can be seen in Fig. 5, where the SIM of the system is plotted for varying L_0 parameter. We set $L_0 = 140$ Henry (H) so that the SIM is not monotonous. On Fig. 6, it is shown that other three electrical components have effects on local extrema, stable and unstable zones of the SIM. This shows that electrical components can be chosen to modify the system behaviour as it will be presented in the next section. It is also noted that if the linear part of the electrical equation is negative ($\Theta_V > 0$), a bistable situation can arise [50]. Figure 7 depicts phase portraits of $Q(t^*)$ which are obtained by direct numerical integration of Eq. 9, for $\zeta = -1$. Time responses of r_2, r_3 and Q are presented in the Fig. 8. It is seen that the system with coupled circuits which posses a negative linear part can present chaotic behaviour, while the same system without coupled circuits presents a quasi-periodic response. Thus, the electrical components can lead to the creation of particular regimes for the electromechanical system. In the next section some numerical results will be presented showing periodic and non periodic responses of the system.

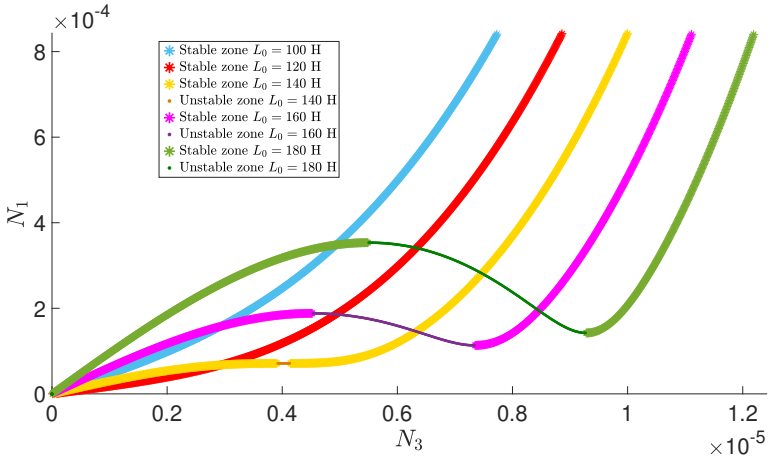

Fig. 5 The SIM (see Eq. 34) of the system for different values of the inductance L_0.

4.2 Numerical examples: equilibrium points according to the forcing amplitude

Depending on the amplitude of external excitation, the system can be attracted by periodic regimes (stable or unstable) presenting different amplitude/ energy levels of system variables. It can also reach to quasi-periodic regimes due to the existence of singularities [51]. In order to study different possible scenarios, equilibrium points of the system are traced versus the amplitude of the external force F, see Figs. 9 and 11. These figures are obtained for the same set of electrical parameters but for different values of ν: $\nu = 1$ (see Fig. 9) and $\nu = 1.01$ (see Fig. 11). Stabilities of equilibrium points are revealed by examining the eigenvalues of the matrices $\boldsymbol{C}$ and $\boldsymbol{J}_1^{-1}\boldsymbol{M}^*$ of Eqs. 40, 43 and 44. A zoomed area of Fig. 9 is illustrated in Fig. 10, showing that the unstable zone at t_0 time scale is very narrow (see the gap between F_- and F_+ in Fig. 10). For certain ranges of forcing amplitude, different dynamics are spotted:

- For $\nu = 1$ and $F < F_{e,-}$ periodic solutions on the lower branch can be observed while for $F > F_{e,+}$ periodic solutions are located on the upper branch.
- For $\nu = 1$ and $F_- < F < F_+$ stable periodic solutions are positioned on the upper branch, and two unstable solutions are placed on the lower and middle branches.
- For $\nu = 1.01$, unstable periodic solution leading to modulated responses should be achieved for 5×10^{-6} m$< F < 8 \times 10^{-6}$m.

In order to validate these predictions, in the next section the three-dimension SIM is confronted with results obtained from direct numerical integration of system equation for chosen forcing amplitudes.

4.3 Confronting the SIM with numerical results

Several dynamical behaviours are awaited from the analysis of Figs. 9 and 11. First, let us trace a periodic stable solution for the system with $\nu = 1$ and $F =$

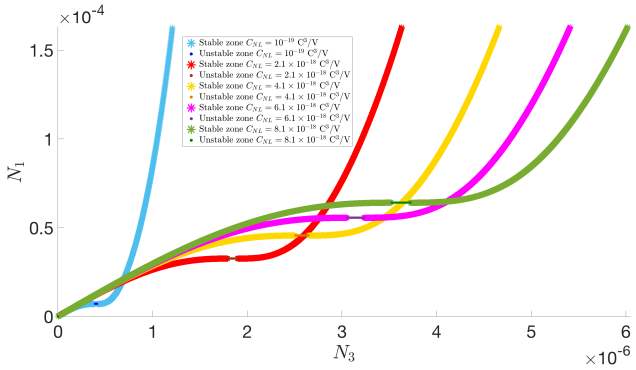

(a) The SIM of the system for varying C_{NL}

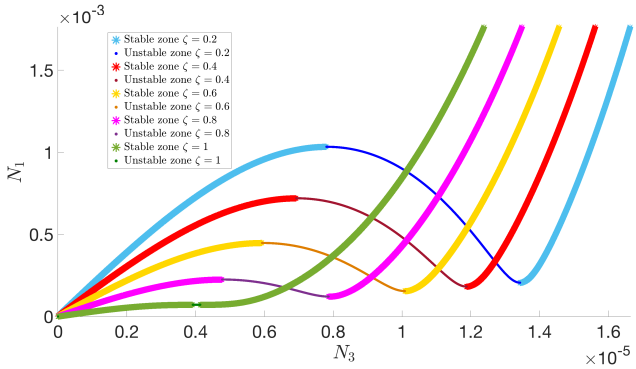

(b) The SIM of the system for varying ζ

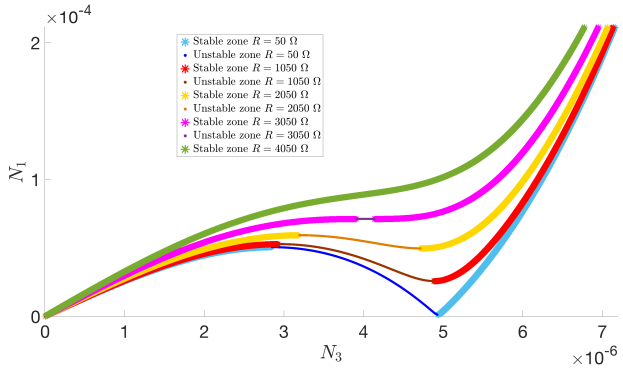

(c) The SIM of the system for varying R

Fig. 6 The SIM of the system for different values of the electrical components: the resistance R, the nonlinear capacitance C_{NL} and the coefficient ζ.

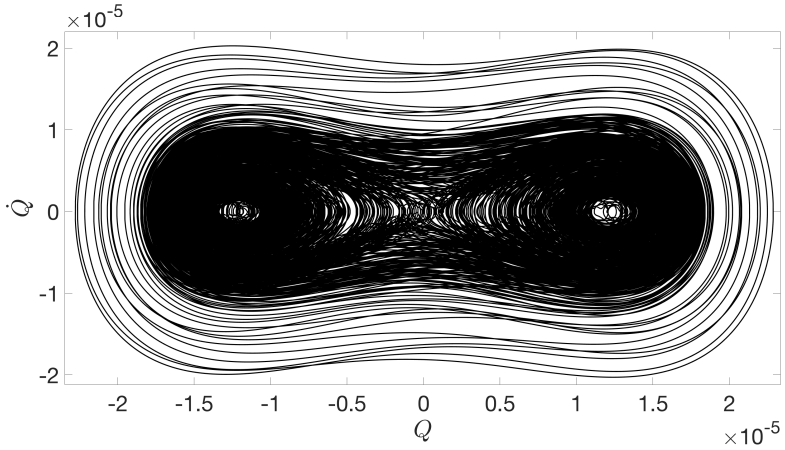

Fig. 7 Phase portrait traced from the numerical integration of Eq. 9, for $\zeta = -1$, $L_0 = 140$ H, $C_{NL} = 10^{-17}$ C^3.V, $R = 3050\ \Omega$ and $F = 7.5 \times 10^{-6}$ m.

$5 \times 10^{-6}\ m$, with zero initial conditions (for all system variables and their first derivatives). It can be seen that even though the lower equilibrium point for $\nu = 1$ is unstable at t_0, it leads to a quasi-periodic behaviour for, see Fig. 12. With higher initial conditions, such as $r_n(0) = 6 \times 10^{-4}$ and all others to be set to 0, the dynamics is attracted by the highest equilibrium point which is stable, leading to a periodic behaviour as illustrated in Fig. 13. The system presents a modulated response for $\nu = 1.01$ and an amplitude of forcing F for which there is only one unstable equilibrium point, see Fig. 14. To verify those regimes, time responses of $r_n(t^*)$ corresponding to different cases which are shown in Figs. 12, 13 and 14 are illustrated in Fig. 4.3. From Figs. 15(a) and 15(c), quasi-periodic regimes are identified. This behaviour can be seen for other variables $r_m(t^*)$ and $q(t^*)$. These reponses are due to the fact that the equilibrium points are situated in the vicinity of singular points (Eq. 45), see Figs. 12 and 14.
From Fig. 14, it can be seen that results obtained by direct numerical integration of system equations are qualitatively following the SIM and they are attracted by the analytically predicted equilibrium points. A quantitative difference can be observed for the variable N_2. This can be due to the effect of the first harmonic which is not taken into account for this variable (see Eq. 28). Nevertheless, analytical results provide a qualitatively good estimation of the system behaviour.
In the next subsection, the frequency response curves of the system for sweeping ν are presented and commented on.

4.4 Numerical results: tracing analytical frequency response curves

From the analytical expression, it is possible to obtain the periodic solutions (see Eqs. 30 and 32) and to judge on their stabilities (see Eq. 40) for a sweeping frequency ν around 1. For the set of parameters used previously and the forcing amplitudes $F = 5 \times 10^{-6}\ m$ and $F = 7.5 \times 10^{-6}\ m$, the frequency responses are depicted in Figs. 16 and 17. The whole behaviours around the lower frequency

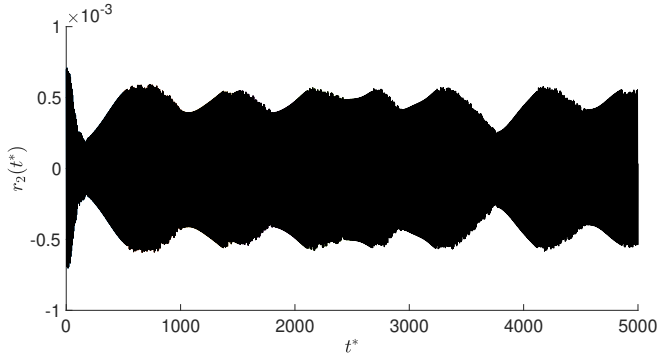

(a) Time response of $r_2(t^*)$

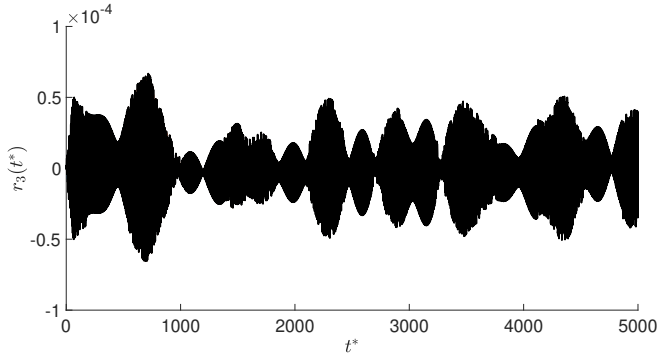

(b) Time response of $r_3(t^*)$

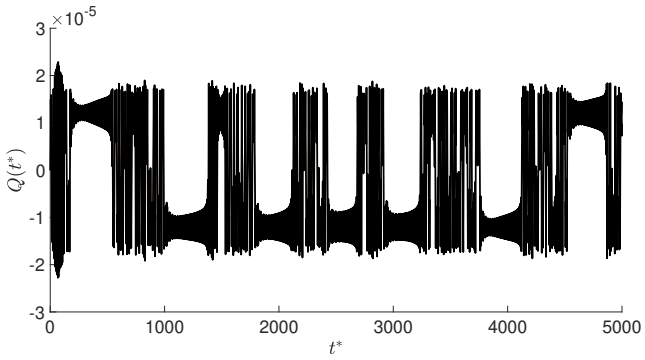

(c) Time response of $Q(t^*)$

Fig. 8 Time history of system variables while the charge Q presents a chaotic behaviour. The electrical components are $\zeta = -1$, $L_0 = 140$ H, $C_{NL} = 10^{-17}$ C^3.V, $R = 3050$ Ω. The amplitude of forcing is $F = 7.5 \times 10^{-6}$ m.

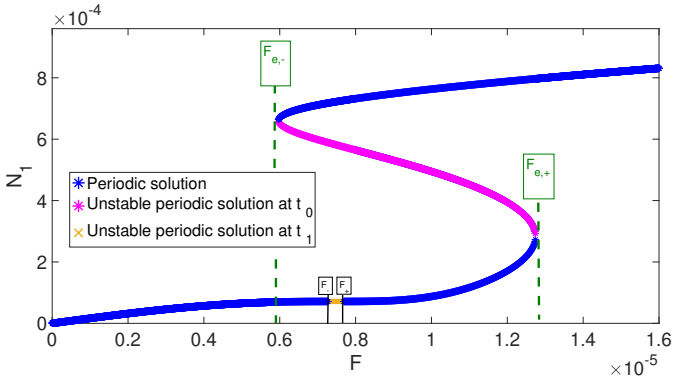

(a) Equilibrium points: N_1 according to F

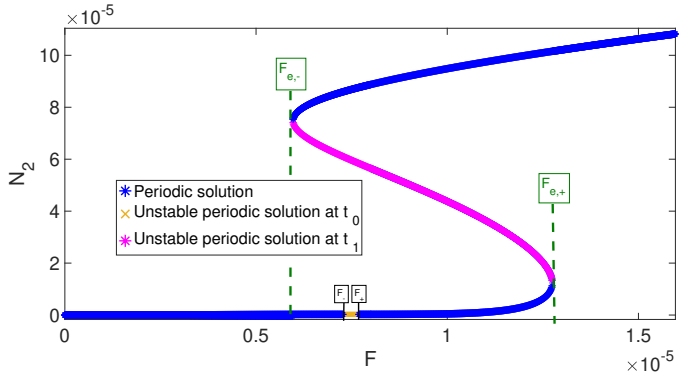

(b) Equilibrium points: N_2 according to F

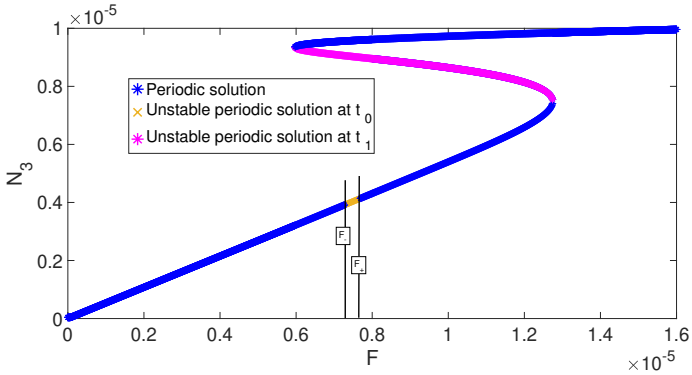

(c) Equilibrium points: N_3 according to F

Fig. 9 Equilibrium points found from Eq. 37, accompanied by their stability analyses at different time scales obtained from Eqs. 40 and 42, $R = 3050\ \Omega$, $L_0 = 140\ H$, $C_{NL} = 10^{-17}\ C^3/V$, $\nu = 1$. $F_\pm$ are traced from Eq. 45.

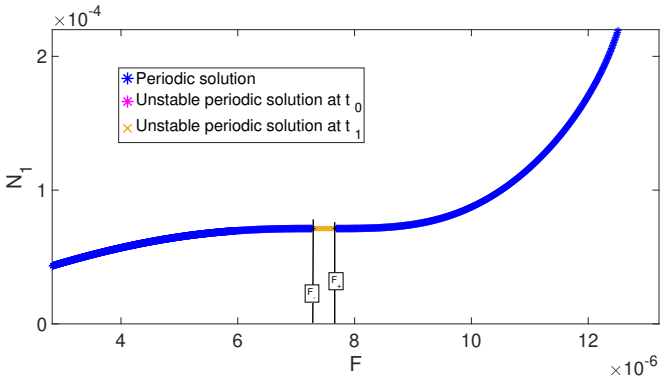

Fig. 10 Equilibrium points detected by Eq. 37, accompanied by their stability analyses at different time scales obtained from Eqs. 40 and 42 with $R = 3050\ \Omega$, $L_0 = 140\ H$, $C_{NL} = 10^{-17}\ C^3/V$, $\nu = 1.F_{\pm}$ are traced from Eq. 45. This figure is a zoom of Fig. 9 where there are unstable periodic solutions.

ω_n can be studied for the non dimensionalized system. For $F = 5 \times 10^{-6}$ on the Fig. 16, stable and unstable characteristic points lead the system to periodic and quasi-periodic behaviours which stay under a threshold of $N_1 = 10^{-4}$. On the other hand, for $F = 7.5 \times 10^{-6}\ m$ in Fig. 17, the apparition of an isola can lead to high amplitudes of N_1 while staying under a threshold of $N_1 = 1.2 \times 10^{-3}$. Thus, the frequency response curves are important for identifying different ranges of system amplitudes for the sweeping frequency. In order to confirm analytical predictions, a numerical integration is carried out for $F = 7.5 \times 10^{-6}\ m$ and obtained results are compared with analytical solutions. From obtained results by numerical integration, the maximum values of the last thirty period are collected for N_1, N_2 and N_3. This is why there are small discrepancies between numerical and analytically predicted results. In fact, obtained results from numerical integrations show that for the especial zone, system presents quasi-periodic responses. From Fig. 18, it is observed that the amplitude of N_1 stays under a threshold even with unstable periodic solutions. This behaviour is due to using the nonlinear circuit which is interesting from passive control viewpoint as it allows (via tuning its parameters properly) the response of the system stays below a given threshold. Meanwhile, if initial conditions are high enough, the stable solution can be found on the isola. This is why the response of the system should be predicted and detected completely (e.g. the case of existence of an isola) for preventing that the system presents unwanted/uncontrolled responses. It can be seen that for N_1 and N_3 the analytical and numerical results are qualitatively in good agreements, which is not the case for N_2. This phenomena can be explained by the fact that the influence of the first harmonic is important for the variable r_m.
In the next subsection a comparison of system responses between the one equipped with the nonlinear and linear circuits are presented. The latter corresponds to a resonant circuit.

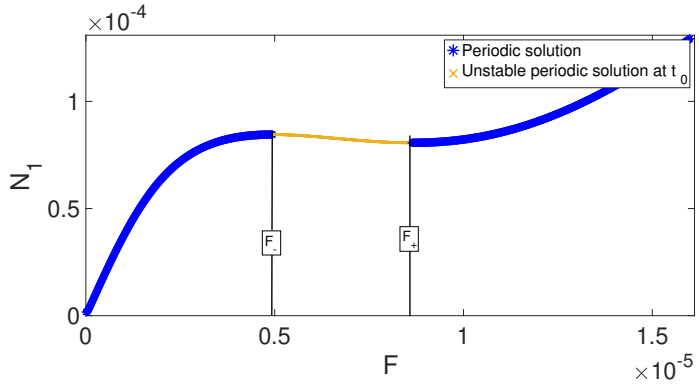

(a) Equilibrium points: N_1 according to F

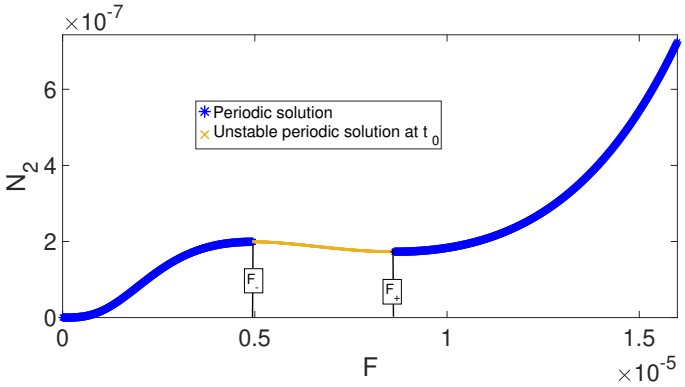

(b) Equilibrium points: N_2 according to F

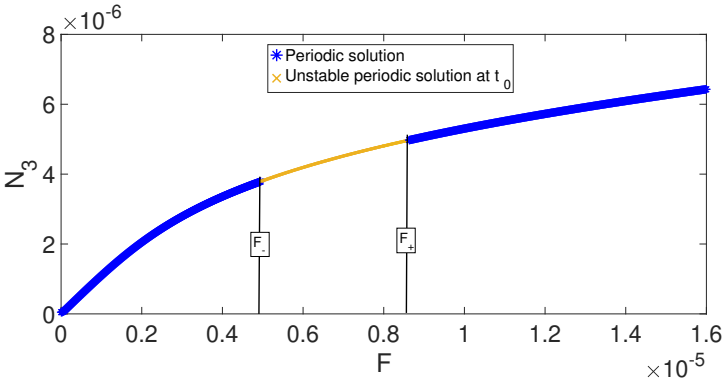

(c) Equilibrium points: N_3 according to F

Fig. 11 Equilibrium points detected by Eq. 37, accompanied by their stability analyses at different time scales obtained from Eqs. 40 and 42. $R = 3050\ \Omega$, $L_0 = 140\ H$, $C_{NL} = 10^{-17}\ C^3/V$, $\nu = 1.01$.

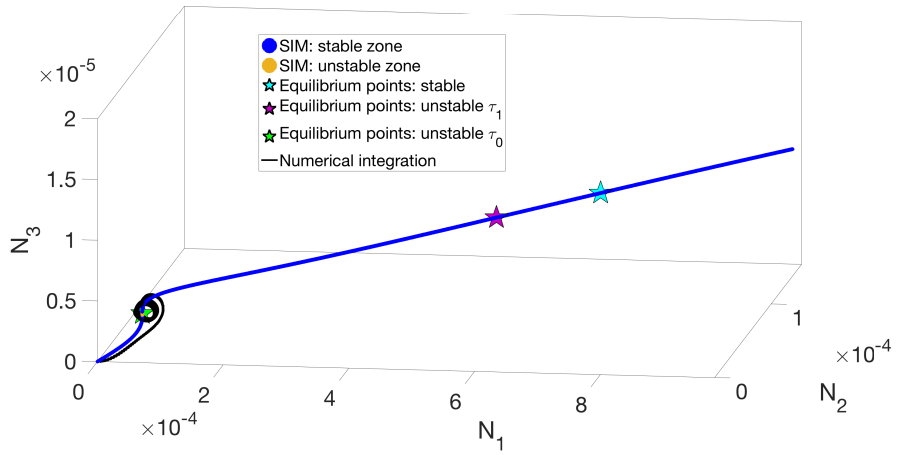

(a) Three dimensional SIM with its three equilibrium points

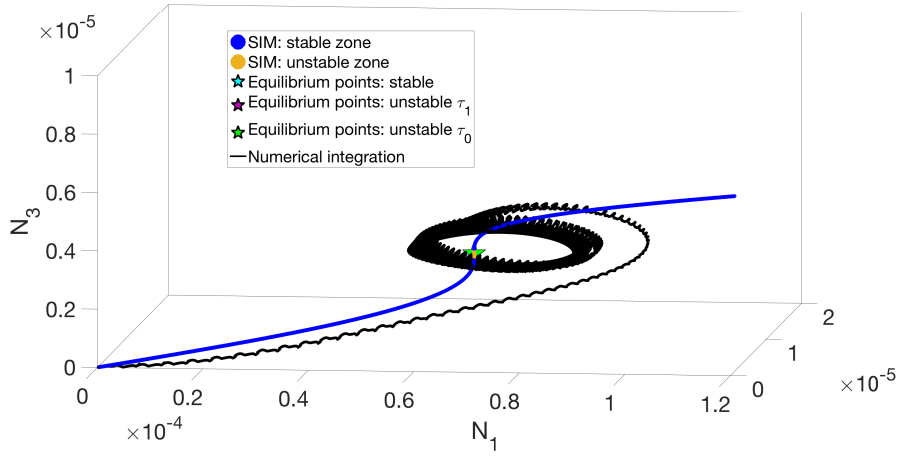

(b) Zoom on the lower equilibrium point

Fig. 12 The SIM is traced from Eq. 34 with its stability calculated from Eq. 35, for $R = 3050\ \Omega$, $L_0 = 140\ H$ and $C_{NL} = 10^{-17}\ C^3/V$. The forcing amplitude and driving frequency are $F = 5 \times 10^{-6}\ m$ and $\nu = 1$, respectively. Equilibrium points are identified through Eq. 37 and their stable and unstable zones are clarified from Eqs. 40 and 42.The initial conditions are set to zero for the numerical integration of Eq. 9.

4.4.1 Comparison between analytical and numerically obtained frequency response curves

To verify the advantages of using a nonlinear circuit compared to a linear resonant one, the frequency response curves are traced numerically for a set of electrical parameters for the nonlinear circuit. The frequency of the resonant circuit is tuned to match the frequency of the main structure, see Fig. 19. Due to the set of electrical parameter, apart from the isola, the frequency response curve of the nonlinear circuit stays under the one of the resonant circuit. This proves that

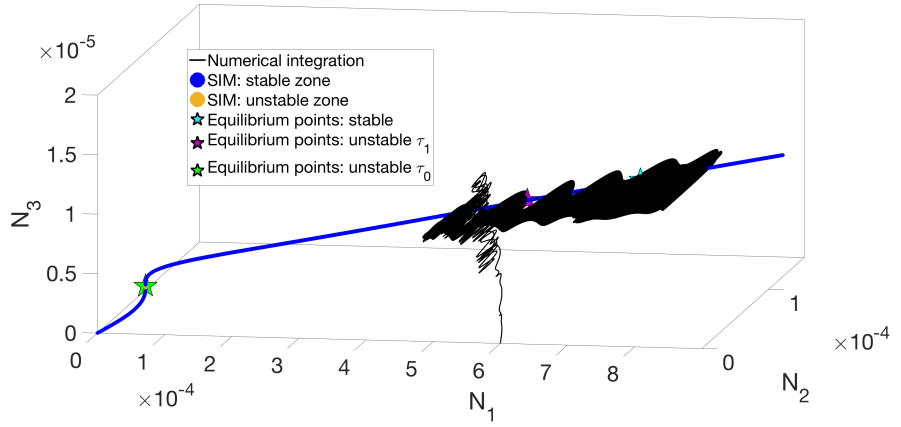

Fig. 13 The SIM is traced from Eq. 34 with its stability calculated from Eq. 35, for$R = 3050\ \Omega$, $L_0 = 140\ H$ and $C_{NL} = 10^{-17}\ C^3/V$. The forcing amplitude and driving frequency are $F = 7.5 \times 10^{-6}\ m$ and $\nu = 1$, respectively. Equilibrium points are identified through Eq. 37 and their stability-unstability zones are clarified from Eqs. 40 and 42. Initial conditions are $x(0) = 6 \times 10^{-4}$ and the rest equal to zero for the numerical integration of Eq. 9.

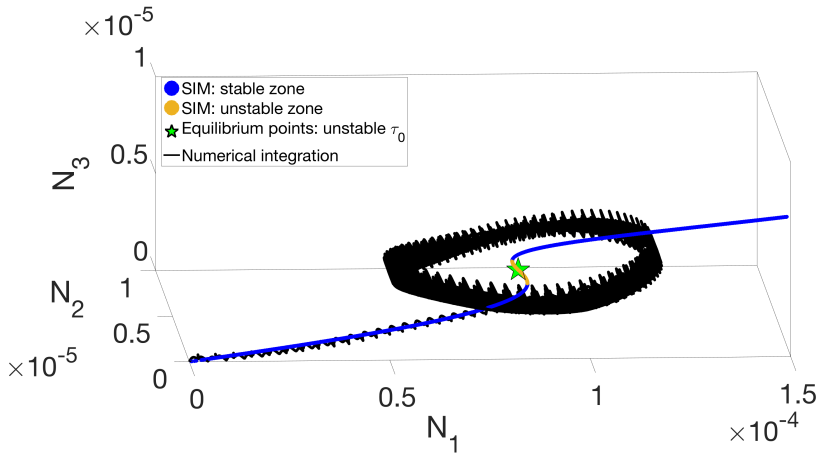

Fig. 14 The SIM is traced from Eqs. 30 and 32 with its stability calculated from Eq. 35, for $R = 3050\ \Omega$, $L_0 = 140\ H$ and $C_{NL} = 10^{-17}\ C^3/V$, and $\nu = 1.01$. Equilibrium points are identified through Eq. 37 and their stability-unstability zones are clarified from Eqs. 40 and 42. The initial conditions are the origin for the numerical integration of Eq. 9.

the nonlinear circuit can be optimized in order to control the vibrations of the beam. On the other hand, being on the isola of the frequency response curves can improve harvesting the energy of the electrical circuit (with N_3). The behaviours of the electromechanical systems (with two types of circuits: nonlinear and linear) are compared with those of the homogeneous beam (i.e. the beam without any piezoelectric patches). It can be seen that the electrical circuits contributes to reduction of the vibration levels of the structure (apart from the isola). In order to

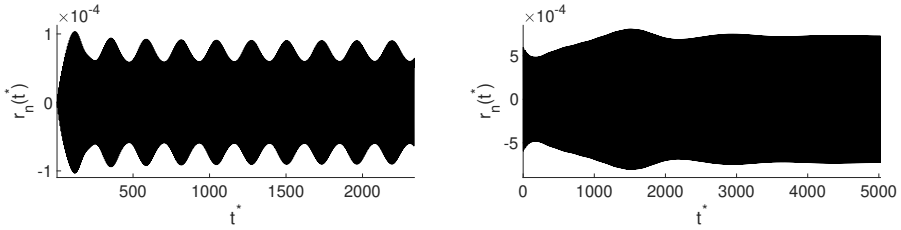

(a) Time history of r_n corresponding to Fig. 12. Quasi-periodic regime.

(b) Time history of r_n corresponding to Fig. 13. Periodic regime.

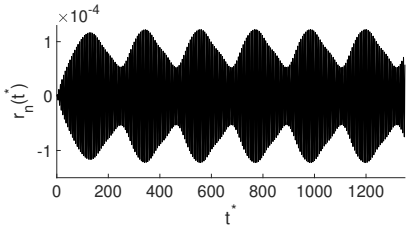

(c) Time history of $_n$ corresponding to Fig. 14. Quasi-periodic regime.

Fig. 15 Time history of of $r_n(t^*)$ traced from the numerical integration of Eq. 9 for the parameters of a) Fig. 12, b) Fig. 13 and c) Fig. 14.

verify the results in the time domain, for a given ν (e.g. $\nu = 1.02$), time histories of $r_n(t^*)$, $r_m(t^*)$ and $q(t^*)$ are depicted in Fig. 20. It is seen that:

- the nonlinear and resonant circuits reduce the vibration levels of the system compared to an open circuit condition or a beam without piezoelectric materials.
- the nonlinear and resonant circuit improves the energy exchange between the n^{th} and the m^{th} mode (increasing the amplitude of $r_m(t^*)$.

If the value of the inductance is modified, it is possible to damp the vibration of the two mechanical modes (see Fig. 21) with $L_0 = 66\ H$. Thus, the nonlinear circuit can be used to damp the vibrations of the two mechanical modes. It shows that via tuning values of the electrical components, it is also possible balance the energies of the two internally resonant modes.

5 Conclusion

An internally resonant composite beam which consists of a homogeneous nonlinear beam patched with a piezoelectric material on it which is linked to a nonlinear circuit, is investigated. The structure is designed so that two modes are in internal resonance: as an example a $1:3$ resonance in this work. Revealing fast and slow system dynamics permits to detect slow invariant manifold and characteristic points, i.e. equilibrium points and fold singularities, of the dynamical system. It is shown that the parameters of the nonlinear circuit can change the behaviour

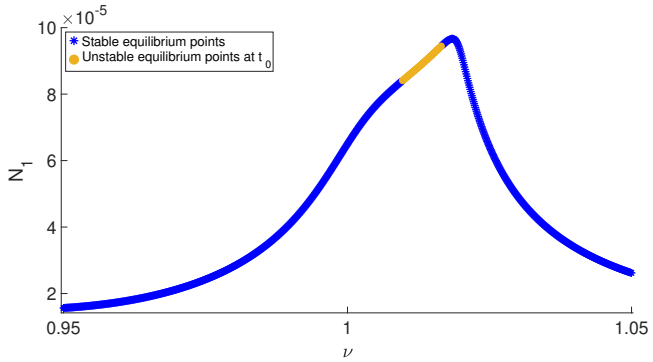

(a) Analytical frequency response of N_1

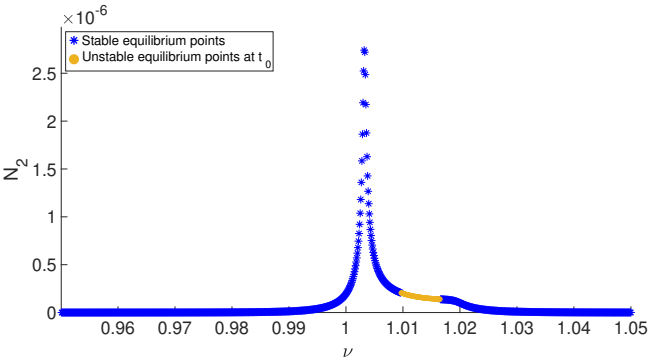

(b) Analytical frequency response of N_2

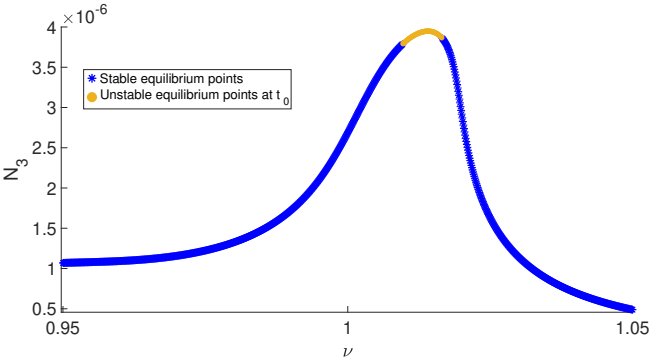

(c) Analytical frequency response of N_3

Fig. 16 Frequency response curves (equilibrium points) found from Eq. 37 with their stability analyses calculated from Eqs. 40 and 42, for the set of following electrical parameters: $R = 3050\ \Omega$, $L_0 = 140\ H$, $C_{NL} = 10^{-17}\ C^3/V$ and the forcing amplitude $F = 7.5 \times 10^{-6}\ m$.

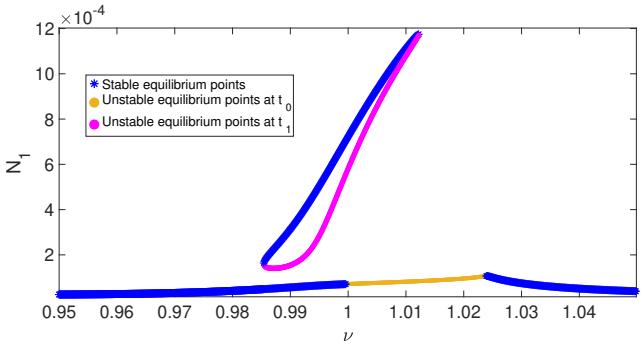

(a) Analytical frequency response of N_1

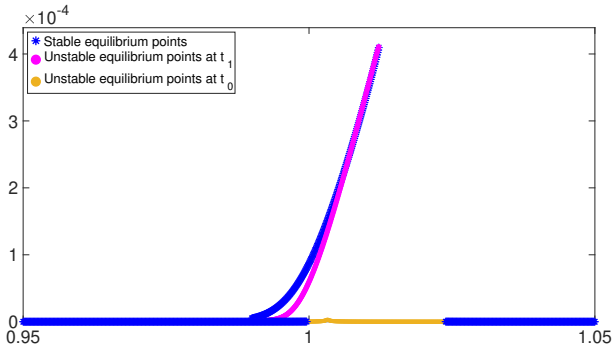

(b) Analytical frequency response of N_2

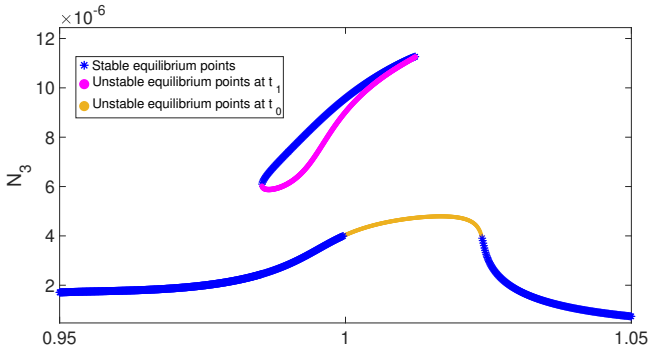

(c) Analytical frequency response of N_3

Fig. 17 Frequency response curves (equilibrium points) found from Eq. 37 with their stability analyses calculated from Eqs. 40 and 42, for the set of following electrical parameters: $R = 3050\ \Omega$, $L_0 = 140\ H$, $C_{NL} = 10^{-}17\ C^3/V$ and the forcing amplitude $F = 7.5 \times 10^{-6}\ m$.

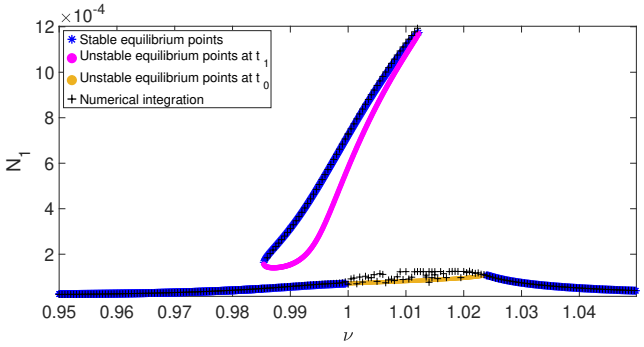

(a) Frequency response of N_1

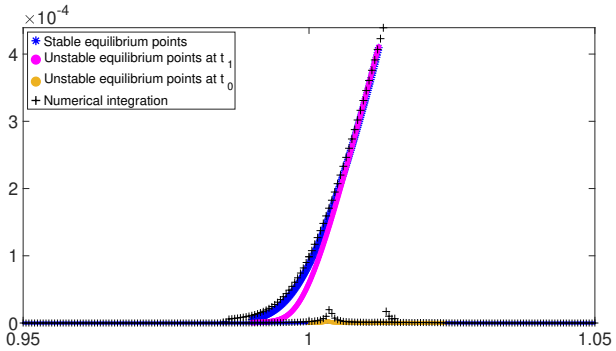

(b) Frequency response of N_2

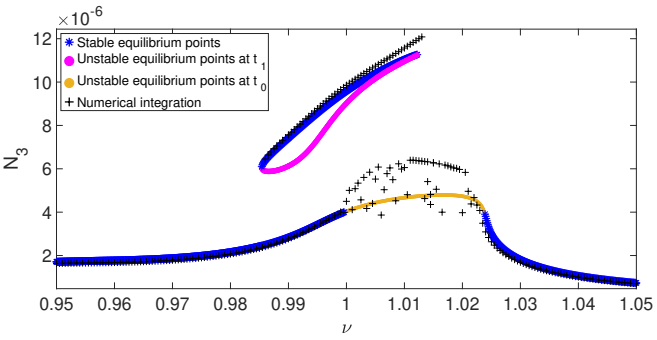

(c) Frequency response of N_3

Fig. 18 Frequency response curves for $R = 3050\ \Omega$, $L_0 = 140\ H$, $C_{NL} = 10^{-17}\ C^3/V$ and the forcing amplitude $F = 7.5 \times 10^{-6}\ m$, obtained from analytical method ('*') (see Eq. 37) with their stability (blue '*') and instability (red 'o') (see Eq. 42) and numerical integration of Eq. 9 (black '+').

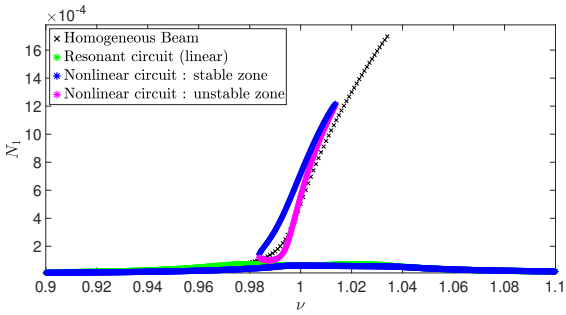

(a) Frequency response of a nonlinear and a resonant circuit for N_1

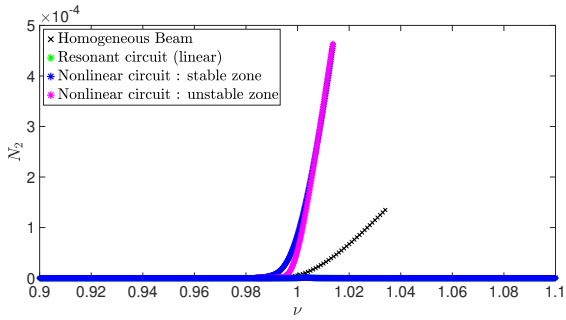

(b) Frequency response of a nonlinear and a resonant circuit for N_2

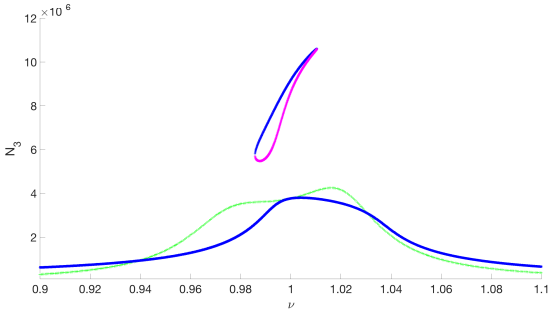

(c) Frequency response of a nonlinear and a resonant circuit for N_3

Fig. 19 Comparison of frequency response curves for $F = 7 \times 10^{-6}$ m of a resonant and nonlinear circuit, with the electrical parameters of the nonlinear circuit as $R = 3050$ Ω, $L_0 = 22$ H, $\mu = 0.1$,$C_{NL} = 10^{-17}$ C^3/V.

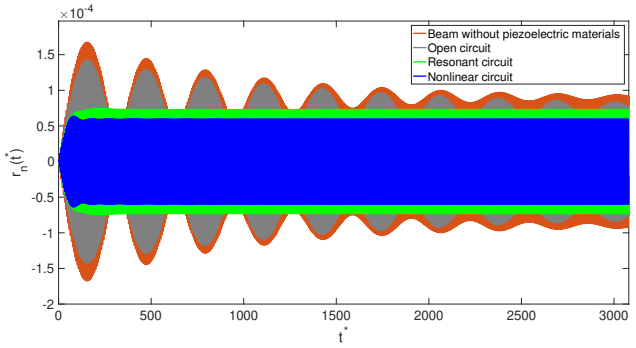

(a) Time response of the variable $r_n(t^*)$

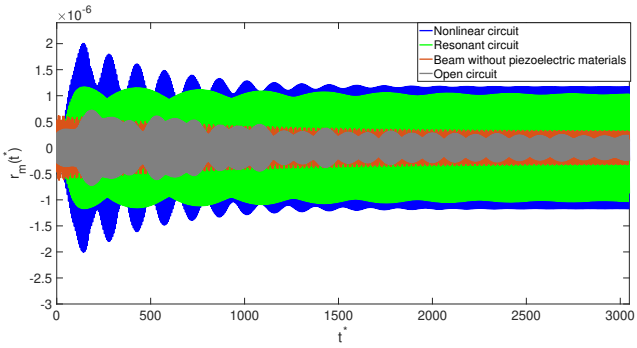

(b) Time response of the variable $r_m(t^*)$

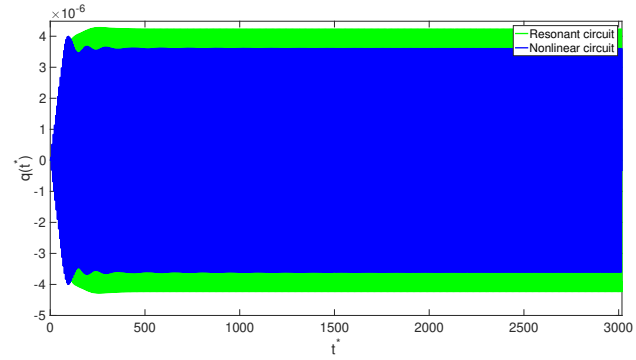

(c) Time response of the variable $q(t^*)$

Fig. 20 Time histories of system variables, with the electrical parameters of the nonlinear circuit as $R = 3050\ \Omega$, $L_0 = 22\ H$, $\mu = 0.1$,$C_{NL} = 10^{-17}\ C^3/V$, for $\nu = 1.02$. This comparison is carried out with a beam without piezoelectric materials and with one piezoelectric material link to: - no circuit (open circuit condition), a resonant circuit and a nonlinear circuit.

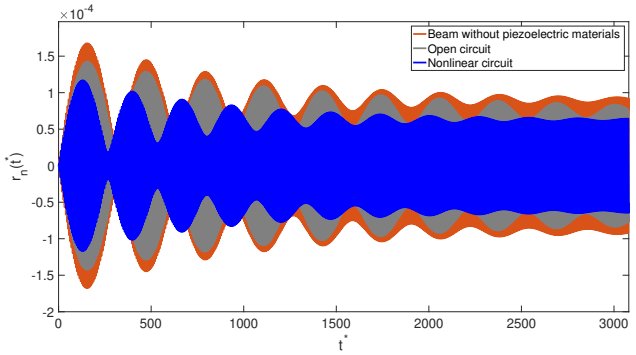

(a) Time response of the variable $r_n(t^*)$

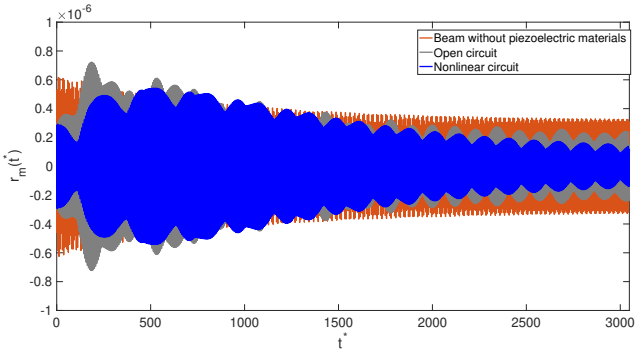

(b) Time response of the variable $r_m(t^*)$

Fig. 21 Time histories of system variables, with the electrical parameters of the nonlinear circuit as $R = 3050\ \Omega$, $L_0 = 66\ H$, $\mu = 0.1$,$C_{NL} = 10^{-17}\ C^3/V$, for $\nu = 1.02$. This comparison is carried out with a beam without piezoelectric materials and with one piezoelectric material link to: - no circuit (open circuit condition) and a nonlinear circuit.

of internally resonant modes via altering their energies and acting as an auto-equilibrator of modal energies of resonant modes during periodic or non-periodic regimes. This phenomena is due to strong modification of the nonlinear interactions between modes, bridged by the nonlinear circuit. It is also seen that the frequency response curves of the system can presents isola which should not be ignored in designing of such systems as they can correspond to high levels of modal energies. It is spotted that different parameters can lead the system to present periodic, quasi-periodic and even chaotic responses. The idea is to "design" (or to master) inter-modal energy exchanges between two resonant modes of a beam via using a nonlinear circuit. The global idea is to design (or tune) such nonlinearity for the global aim which can be desired final periodic or non periodic regimes. The developed techniques provide design tools for tuning parameters of the nonlinear circuit and also selection of adapted piezoelectric material.
One of outlooks of this work will be finite element modelling of the system under consideration and design of an experimental system with developed techniques in this paper, to verify analytical predictions with results of finite element modelling

and experimentations. Other perspective of this work is also the optimization of the nonlinear circuit via taking into account the permitted modal energies thresholds for given width of excitation characteristics, i.e. frequency and amplitude. The optimization can be made either to obtain improved energy harvesting or mitigation of vibratory energies of the electromechanical beam. Other internal resonance cases could be studied for this system, or taking into account several internal resonances involved in the system dynamics.

Acknowledgements The authors would like to thank following organizations for supporting this research: i) The "Ministére de la Transition écologique" and ii) LABEX CELYA (ANR-10-LABX-0060) of the "Université de Lyon" within the program "Investissement d'Avenir" (ANR-11-IDEX-0007) operated by the French National Research Agency (ANR).

Conflict of interest

The authors declare that they have no conflict of interest.

A Definition of the parameters of Eqs. 4

The parameters of Eq. 4 are as:

$$
\begin{aligned}
\mu_n = &\quad \int_0^{L_b} c_v \phi_n^2 \; ds \\
\omega_n^2 = &\quad \int_0^{L_b} EI \phi_n^{(iv)}(s) \phi_n \; ds \\
F_n = &\quad \int_0^{L_b} \mu F \phi_n \; ds \\
De_{nnn} = &\quad \int_0^{L_b} (-EI)(\phi_n'(\phi_n'\phi_n'')')' \; \phi_n \; ds \\
De_{nnm} = &\quad \int_0^{L_b} (-EI)(\phi_n'(\phi_m'\phi_n'')' + \phi_n'(\phi_m'\phi_n'')' + \phi_n'(\phi_n'\phi_m'')')' \; \phi_n \; ds \\
De_{nmm} = &\quad \int_0^{L_b} (-EI)(\phi_m'(\phi_m'\phi_n'')' + \phi_n'(\phi_m'\phi_m'')' + \phi_m'(\phi_n'\phi_m'')')' \; \phi_n \; ds \\
De_{mmm} = &\quad \int_0^{L_b} (-EI)(\phi_m'(\phi_m'\phi_m'')')' \; \phi_n \; ds \\
G_{nnn} = &\quad \int_0^{L_b} (\phi_n' \int_s^{L_b} \frac{-\mu}{2} \int_s^0 \phi_n'^2 \; ds \; ds)' \; \phi_n \; ds \\
G_{nnm} = &\quad \int_0^{L_b} (\phi_n' \int_s^{L_b} \frac{-\mu}{2} \int_s^0 \phi_n'\phi_m' \; ds \; ds)' \; \phi_n \; ds \\
G_{nmm} = &\quad \int_0^{L_b} (\phi_n' \int_s^{L_b} \frac{-\mu}{2} \int_s^0 \phi_m'^2 \; ds \; ds)' \; \phi_n \; ds \\
G_{mnn} = &\quad \int_0^{L_b} (\phi_m' \int_s^{L_b} \frac{-\mu}{2} \int_s^0 \phi_n'^2 \; ds \; ds)' \; \phi_n \; ds \\
G_{mnm} = &\quad \int_0^{L_b} (\phi_m' \int_s^{L_b} \frac{-\mu}{2} \int_s^0 \phi_n'\phi_m' \; ds \; ds)' \; \phi_n \; ds \\
G_{mmm} = &\quad \int_0^{L_b} (\phi_m' \int_s^{L_b} \frac{-\mu}{2} \int_s^0 \phi_m'^2 \; ds \; ds)' \; \phi_n \; ds \\
De_V = &\quad -\frac{b_p d_{31}(y_2^2 - y_1^2)}{2h_p} \int_{x_1}^{x_2} \phi_n'' \; ds
\end{aligned}
\tag{46}
$$

$$
\begin{aligned}
\mu_m = &\quad \int_0^{L_b} c_v \phi_m^2 \; ds \\
\omega_m^2 = &\quad \int_0^{L_b} EI \phi_m^{(iv)}(s) \phi_m \; ds \\
F_m = &\quad \int_0^{L_b} \mu F \phi_m \; ds \\
Ae_{nnn} = &\quad \int_0^{L_b} (-EI)(\phi_n'(\phi_n'\phi_n'')')' \; \phi_m \; ds \\
Ae_{nnm} = &\quad \int_0^{L_b} (-EI)(\phi_n'(\phi_m'\phi_n'')' + \phi_n'(\phi_m'\phi_n'')' + \phi_n'(\phi_n'\phi_m'')')' \; \phi_m \; ds \\
Ae_{nnm} = &\quad \int_0^{L_b} (-EI)(\phi_m'(\phi_m'\phi_n'')' + \phi_n'(\phi_m'\phi_m'')' + \phi_m'(\phi_n'\phi_m'')')' \; \phi_m \; ds \\
Ae_{mmm} = &\quad \int_0^{L_b} (-EI)(\phi_m'(\phi_m'\phi_m'')')' \; \phi_m \; ds \\
Ga_{nnn} = &\quad \int_0^{L_b} (\phi_n' \int_s^{L_b} \frac{-\mu}{2} \int_s^0 \phi_n'^2 \; ds \; ds)' \; \phi_m \; ds \\
Ga_{nnm} = &\quad \int_0^{L_b} (\phi_n' \int_s^{L_b} \frac{-\mu}{2} \int_s^0 \phi_n'\phi_m' \; ds \; ds)' \; \phi_m \; ds \\
Ga_{nmm} = &\quad \int_0^{L_b} (\phi_n' \int_s^{L_b} \frac{-\mu}{2} \int_s^0 \phi_m'^2 \; ds \; ds)' \; \phi_m \; ds \\
Ga_{mnn} = &\quad \int_0^{L_b} (\phi_m' \int_s^{L_b} \frac{-\mu}{2} \int_s^0 \phi_n'^2 \; ds \; ds)' \; \phi_m \; ds \\
Ga_{mnm} = &\quad \int_0^{L_b} (\phi_m' \int_s^{L_b} \frac{-\mu}{2} \int_s^0 \phi_n'\phi_m' \; ds \; ds)' \; \phi_m \; ds \\
Ga_{mmm} = &\quad \int_0^{L_b} (\phi_m' \int_s^{L_b} \frac{-\mu}{2} \int_s^0 \phi_m'^2 \; ds \; ds)' \; \phi_m \; ds \\
Ae_V = &\quad -\frac{b_p d_{31}(y_2^2 - y_1^2)}{2h_p} \int_{x_1}^{x_2} \phi_m'' \; ds
\end{aligned}
\tag{47}
$$

The parameters of Eq. 9 are defined as:

$$
\begin{aligned}
a_1 = \quad & \frac{\mu_n}{\omega_n}, \qquad \nu = \quad \frac{\Omega}{\omega_n}, \\
\Lambda_{nnn} = \quad & \frac{De_{nnn}}{\omega_n^2}, \quad \Lambda_{nnm} = \quad \frac{De_{nnm}}{\omega_n^2}, \\
\Lambda_{nmm} = \quad & \frac{De_{nmm}}{\omega_n^2}, \quad \Lambda_{mmm} = \frac{De_{mmm}}{\omega_n^2}, \\
L_{nnn} = \quad & G_{nnn}, \qquad L_{nnm} = \quad G_{nnm}, \\
L_{nmm} = \quad & G_{nmm}, \qquad L_{mnn} = \quad G_{mnn}, \\
L_{mnm} = \quad & G_{mnm}, \qquad L_{mmm} = G_{mmm}, \\
\gamma_V = \quad & \frac{De_V}{L_V \omega_n^2}, \\
\gamma_n = \quad & -\frac{De_V L_n}{L_V \omega_n^2}, \; \gamma_m = \quad -\frac{De_V L_m}{L_V \omega_n^2}
\end{aligned}
\tag{48}
$$

$$
\begin{aligned}
a_2 = \quad & \frac{\mu_m}{\omega_m}, \qquad \Gamma_{nnn} = \quad \frac{Ae_{nnn}}{\omega_n^2}, \\
\Gamma_{nnm} = \quad & \frac{Ae_{nnm}}{\omega_n^2}, \quad \Gamma_{nmm} = \quad \frac{Ae_{nmm}}{\omega_n^2}, \\
T_{nnn} = \quad & Ga_{nnn}, \qquad T_{nnm} = \quad Ga_{nnm}, \\
T_{nmm} = \quad & Ga_{nmm}, \qquad T_{mnn} = \quad Ga_{mnn}, \\
T_{mnm} = \quad & Ga_{mnm}, \qquad T_{mmm} = Ga_{mmm}, \\
\Gamma_{mmm} = \quad & \frac{Ae_{mmm}}{\omega_n^2}, \\
\beta_V = \quad & \frac{De_V}{L_V \omega_n^2}, \qquad \beta_n = \quad -\frac{De_V L_n}{L_V \omega_n^2}, \\
\beta_m = \quad & -\frac{De_V L_m}{L_V \omega_n^2}, \; a_3 = \quad \frac{R}{L_0 \omega_n}, \\
\gamma = \quad & \frac{1}{C_{NL} L_0 \omega_n^2}, \; \Theta_V = \quad \frac{1}{L_V L_0 \omega_n^2} - \frac{1}{C_{neg} L_0 \omega_n^2}, \\
\Theta_n = \quad & -\frac{L_n}{L_V L_0 \omega_n^2}, \; \Theta_m = \quad -\frac{L_m}{L_V L_0 \omega_n^2}
\end{aligned}
\tag{49}
$$

It is noted $\zeta = 1 - \dfrac{L_V}{C_{neg}}$ as $\Theta_V = \dfrac{\zeta}{L_V L_0 \omega_n^2}$.

B Definition of the matrix $\boldsymbol{A}$ from Eq. 39

$$
\boldsymbol{A} = \begin{pmatrix}
\dfrac{\partial \mathcal{F}(\phi, \overline{\phi}, \psi, \overline{\psi})}{\partial \phi} & \dfrac{\partial \mathcal{F}(\phi, \overline{\phi}, \psi, \overline{\psi})}{\partial \overline{\phi}} \\
\dfrac{\partial \overline{\mathcal{F}}(\phi, \overline{\phi}, \psi, \overline{\psi})}{\partial \phi} & \dfrac{\partial \overline{\mathcal{F}}(\phi, \overline{\phi}, \psi, \overline{\psi})}{\partial \overline{\phi}}
\end{pmatrix}
\tag{50}
$$

C Definition of the matrices M_j with $j = 1, ..., 5$ from Eq. 41

$$\boldsymbol{M_1} = \begin{pmatrix} \dfrac{\partial \mathcal{G}}{\partial \phi} & \dfrac{\partial \mathcal{G}}{\partial \overline{\phi}} \\ \dfrac{\partial \overline{\mathcal{G}}}{\partial \phi} & \dfrac{\partial \overline{\mathcal{G}}}{\partial \overline{\phi}} \end{pmatrix} \tag{51}$$

$$\boldsymbol{M_2} = \begin{pmatrix} \dfrac{\partial \mathcal{G}}{\partial \phi_3} & \dfrac{\partial \mathcal{G}}{\partial \overline{\phi}_3} \\ \dfrac{\partial \overline{\mathcal{G}}}{\partial \phi_3} & \dfrac{\partial \overline{\mathcal{G}}}{\partial \overline{\phi}_3} \end{pmatrix} \tag{52}$$

$$\boldsymbol{M_3} = \begin{pmatrix} \dfrac{\partial \mathcal{G}}{\partial \psi} & \dfrac{\partial \mathcal{G}}{\partial \overline{\psi}} \\ \dfrac{\partial \overline{\mathcal{G}}}{\partial \psi} & \dfrac{\partial \overline{\mathcal{G}}}{\partial \overline{\psi}} \end{pmatrix} \tag{53}$$

$$\boldsymbol{M_4} = \begin{pmatrix} \dfrac{\partial \mathcal{H}}{\partial \phi} & \dfrac{\partial \mathcal{H}}{\partial \overline{\phi}} \\ \dfrac{\partial \overline{\mathcal{H}}}{\partial \phi} & \dfrac{\partial \overline{\mathcal{H}}}{\partial \overline{\phi}} \end{pmatrix} \tag{54}$$

$$\boldsymbol{M_5} = \begin{pmatrix} \dfrac{\partial \mathcal{H}}{\partial \phi_3} & \dfrac{\partial \mathcal{H}}{\partial \overline{\phi}_3} \\ \dfrac{\partial \overline{\mathcal{H}}}{\partial \phi_3} & \dfrac{\partial \overline{\mathcal{H}}}{\partial \overline{\phi}_3} \end{pmatrix} \tag{55}$$

References

1. P.F. Pai, B. Wen, A.S. Naser, and M.J. Schulz. Structural vibration control using pzt patches and non-linear phenomena. *Journal of Sound and Vibration*, 215(2):273 – 296, 1998.
2. H Li, S Preidikman, B Balachandran, and C D Mote. Nonlinear free and forced oscillations of piezoelectric microresonators. *Journal of Micromechanics and Microengineering*, 16(2):356–367, jan 2006.
3. K. Mam, M. Peigney, and D. Siegert. Finite strain effects in piezoelectric energy harvesters under direct and parametric excitations. *Journal of Sound and Vibbration*, 389:411–437, 2017.
4. P. F. Pai and A. H. Nayfeh. Three-dimensional nonlinear vibrations of composite beams-ii. flapwise excitations. *Nonlinear Dynamics*, 2:1–34, 1991.
5. P. F. Pai and A. H. Nayfeh. Three-dimensional nonlinear vibrations of composite beams-iii. chordwise excitations. *Nonlinear Dynamics*, 2:137–156, 1991.
6. Ali Nayfeh and B. Balachandran. Modal interactions in dynamical and structural systems. *Applied Mechanics Reviews - APPL MECH REV*, 42, 11 1989.
7. C.L. Zaretzky and M.R.M.Crespo da Silva. Experimental investigation of non-linear modal coupling in the response of cantilever beams. *Journal of Sound and Vibration*, 174(2):145 – 167, 1994.
8. Hanna Cho, Bongwon Jeong, Min-Feng Yu, Alexander F. Vakakis, D. Michael McFarland, and Lawrence A. Bergman. Nonlinear hardening and softening resonances in micromechanical cantilever-nanotube systems originated from nanoscale geometric nonlinearities. *International Journal of Solids and Structures*, 49(15):2059 – 2065, 2012.
9. A.D. Shaw, T.L. Hill, S.A. Neild, and M.I. Friswell. Periodic responses of a structure with 3:1 internal resonance. *Mechanical Systems and Signal Processing*, 81:19–34, 2016.

10. M.R.M. Crespo Da Silva. Non-linear flexural-flexural-torsional-extensional dynamics of beams - i.formulation. *The Aerospace Corporation, El-Segundo, TOR-158(3107-18), California*, 24(12):1225–1234, 1988.
11. M. R. M. Crespo Da Silva. Non-linear flexural-flexural-torsional-extensional dynamics of beams-ii. response analysis. *International Journal of Solids and Structures*, 24:1235–1242, 1988.
12. P. F. Pai and A. H. Nayfeh. Three-dimensional nonlinear vibrations of composite beams-i. equations of motion. *Nonlinear Dynamics*, 1:477–502, 1990.
13. Vinciane Guillot, Alireza Ture Savadkoohi, and Claude-Henri Lamarque. Analysis of a reduced order nonlinear model of a multi-physics beam. *Nonlinear Dynamics*, 97(2):1371–1401, 2019.
14. V. Guillot, A. Givois, C. Mathieu, T. Olivier, A. Ture Savadkoohi, and C.-H. Lamarque. Theoretical and experimental investigation of a 1:3 internal resonance in a beam with piezoelectric patches. *Journal of Vibration and Control*, 26(13-14):107754632091053, 2020.
15. U. Andreaus, F. Dell'Isola, and M. Porfiri. Piezoelectric passive distributed controllers for beam flexural vibrations. *Journal of Vibration and Control*, 10(5):625–659, 2004.
16. N.W. Hagood and A. von Flotow. Damping of structural vibrations with piezoelectric materials and passive electrical networks. *Journal of Sound and Vibration*, 146(2):243 – 268, 1991.
17. Yabin Liao and Henry Sodano. Piezoelectric damping of resistively shunted beams and optimal parameters for maximum damping. *Journal of Vibration and Acoustics*, 132, 08 2010.
18. Keisuke Yamada, Hiroshi Matsuhisa, Hideo Utsuno, and Katsutoshi Sawada. Optimum tuning of series and parallel lr circuits for passive vibration suppression using piezoelectric elements. *Journal of Sound and Vibration*, 329(24):5036 – 5057, 2010.
19. Claude Richard, Daniel Guyomar, D. Audigier, and Gil Ching. Semi-passive damping using continuous switching of a piezoelectric device. *Proceedings of SPIE - The International Society for Optical Engineering*, 3672:104–111, 01 1999.
20. Claude Richard, Daniel Guyomar, D. Audigier, and Henri Bassaler. Enhanced semi-passive damping using continuous switching of a piezoelectric device on an inductor. *Smart Structures and Materials: Passive Damping and Isolation, SPIE*, 3989:288–299, 04 2000.
21. A. Badel, G. Sebald, D. Guyomar, M. Lallart, E. Lefeuvre, C. Richard, and J. Qiu. Piezoelectric vibration control by synchronized switching on adaptive voltage sources: Towards wide band semi-active damping. *The Journal of the Acoustical Society of America*, 119, 2006.
22. Elie Lefeuvre, Adrien Badel, Lionel Petit, Claude Richard, and Daniel Guyomar. Semi-passive piezoelectric structural damping by synchronized switching on voltage sources. *Journal of intelligent material systems and structures*, 17:653–660, 08 2006.
23. Boris Lossouarn, Jean-François Deü, and Gaëtan Kerschen. A fully passive nonlinear piezoelectric vibration absorber. *Philosophical Transactions of the Royal Society A: Mathematical, Physical and Engineering Sciences*, 376:20170142, 08 2018.
24. Tarcisio Silva, Marcel Clementino, Carlos De Marqui Jr, and Alper Erturk. An experimentally validated piezoelectric nonlinear energy sink for wideband vibration attenuation. *Journal of Sound and Vibration*, 437:68–78, 12 2018.
25. Joseph J. Hollkamp and Jr Thomas F. Starchville. A self-tuning piezoelectric vibration absorber. *Journal of Intelligent Material Systems and Structures*, 5(4):559–566, 1994.
26. S Behrens, S.O.R Moheimani, and A.J Fleming. Multiple mode current flowing passive piezoelectric shunt controller. *Journal of Sound and Vibration*, 266(5):929–942, 2003.
27. Robert E. Roberson. Synthesis of a nonlinear dynamic vibration absorber. *Journal of the Franklin Institute*, 254(3):205 – 220, 1952.
28. Eugene Sevin. On the Parametric Excitation of Pendulum-Type Vibration Absorber. *Journal of Applied Mechanics*, 28(3):330–334, 09 1961.
29. W. J. Carter and F. C. Liu. Steady-State Behavior of Nonlinear Dynamic Vibration Absorber. *Journal of Applied Mechanics*, 28(1):67–70, 03 1961.
30. R. A. Struble and J. H. Heinbockel. Resonant Oscillations of a Beam-Pendulum System. *Journal of Applied Mechanics*, 30(2):181–188, 06 1963.
31. R. S. Haxton and A. D. S. Barr. The Autoparametric Vibration Absorber. *Journal of Engineering for Industry*, 94(1):119–125, 02 1972.
32. J.B. Hunt and J.-C. Nissen. The broadband dynamic vibration absorber. *Journal of Sound and Vibration*, 83(4):573–578, 1982.

33. H. Kojima and H. Saito. Forced vibrations of a beam with a non-linear dynamic vibration absorber. *Journal of Sound and Vibration*, 88(4):559–568, 1983.
34. F.S. Collette. A combined tuned absorber and pendulum impact damper under random excitation. *Journal of Sound and Vibration*, 216(2):199–213, 1998.
35. AF Vakakis and Oleg Gendelman. Energy pumping in nonlinear mechanical oscillators: Part ii—resonance capture. *Journal of Applied Mechanics-transactions of The Asme - J APPL MECH*, 68, 01 2001.
36. O.V. Gendelman, E. Gourdon, and C.H. Lamarque. Quasiperiodic energy pumping in coupled oscillators under periodic forcing. *Journal of Sound and Vibration*, 294(4):651 – 662, 2006.
37. V. Guillot, A. Ture Savadkoohi, and C.-H. Lamarque. Study of an electromechanical nonlinear vibration absorber: design via analytical approach. *Journal of Intelligent Material Systems and Structures*, 32:410–419, 2021.
38. O. Thomas, J.-F. Deü, and J. Ducarne. Vibrations of an elastic structure with shunted piezoelectric patches: efficient finite element formulation and electromechanical coupling coefficients. *International Journal for Numerical Methods in Engineering*, 80(2):235–268, 2009.
39. Daniel Guyomar, N. Aurelle, and L. Eyraud. Piezoelectric ceramics nonlinear behavior. application to langevin transducer. *Journal de Physique III*, 7:1197–1208, 06 1997.
40. A. Abdelkefi, A.H. Nayfeh, and M.R. Hajj. Global nonlinear distributed-parameter model of parametrically excited piezoelectric energy harvesters. *Nonlinear Dynamics*, 67:1147–1160, 2012.
41. Vinciane Guillot. *Conception multi-échelle de structures électro-mécaniques non linéaires pour le contrôle et la maîtrise des transferts d'énergie*. PhD thesis, NNT: 2020LYSET018, Université de Lyon, December 2020.
42. Ali H. Nayfeh and Dean T. Mook. *Nonlinear Oscillations*. Wiley-VCH, 1995.
43. L.I. Manevitch. The description of localized normal modes in a chain of nonlinear coupled oscillators using complex variables. *Nonlinear Dynamics*, 25(1):95–109, 2001.
44. Diala Bitar, Alireza Ture Savadkoohi, Claude-Henri Lamarque, Emmanuel Gourdon, and Manuel Collet. Extended complexification method to study nonlinear passive control. *Nonlinear Dynamics*, 99, 11 2019.
45. I.T. Georgiou, A.K. Bajaj, and M. Corless. Slow and fast invariant manifolds, and normal modes in a two degree-of-freedom structural dynamical system with multiple equilibrium states. *International Journal of Non-Linear Mechanics*, 33(2):275–300, 1998.
46. Jean-Marc Ginoux, Bruno Rossetto, and Leon O. Chua. Slow invariant manifolds as curvature of the flow of dynamical systems. *International Journal of Bifurcation and Chaos*, 18(11):3409–3430, 2008.
47. Leonid I. Manevitch and Oleg Gendelman. *Tractable models of solid mechanics. Formulation, analysis and interpretation*. Springer-Verlag Berlin Heidelberg, 01 2011.
48. Jean-Marc Ginoux. Slow invariant manifolds of slow–fast dynamical systems. *International Journal of Bifurcation and Chaos*, 31(07):2150112, 2021.
49. Simon Charlemagne, Alireza Ture Savadkoohi, and C.H. Lamarque. Interactions between two coupled nonlinear forced systems: Fast/slow dynamics. *International Journal of Bifurcation and Chaos*, 26, 08 2016.
50. John Guckenheimer and P. J. Holmes. *Nonlinear Oscillations, Dynamical Systems, and Bifurcations of Vector Fields*. Springer-Verlag New York, 1983.
51. Y. Starosvetsky and O.V. Gendelman. Strongly modulated response in forced 2dof oscillatory system with essential mass and potential asymmetry. *Physica D: Nonlinear Phenomena*, 237(13):1719 – 1733, 2008.